The power of modern 3-D visualization of high-resolution terrain models in geologic mapping: Complex fold geometries revealed by 3-D mapping in the Panamint metamorphic complex, eastern California, USA

Terry L. Pavlis and Laura F. Serpa
Department of Earth, Environmental and Resource Sciences, University of Texas at El Paso, El Paso, Texas 79968, USA

ABSTRACT

We use structure from motion– multiview stereo (SM) terrain models developed from ground-based images and images acquired from uncrewed aircraft (aka drones) as a base map for three- dimensional (3-D) mapping on the walls of a deep canyon in the Panamint Range of eastern California, USA. The ability to manipulate the 3-D model with views from arbitrary look directions and broad scale range revealed structures that were invisible to conventional two-dimensional (2-D) mapping because of both the scale of the structures and their exposure on vertical to near-vertical cliff faces. The analysis supports field evidence for four phases of ductile deformation, with only one of the younger phases documented on early geologic maps of the area. The oldest deformational event (D1) produced the main metamorphic fabric and pre-dates Late Cretaceous plutons. This deformation produced a 200–250-m- thick high- strain zone localized along marbles at the top of the Kingston Peak Formation and lower Noonday Formation. Geometric analysis from the model suggests strongly that large sheath folds at scales of 100–300 m are developed within these marbles. Large measured finite strains indicate displacement across this apparent shear zone of at least 4–5 km and displacements of tens of kilometers are allowable, yet the structure is invisible to conventional mapping because the high- strain zone is stratabound. The main fabric shows two clear overprints and a third that is likely an even younger deformation. D2 and D3 generated tight to close, recumbent folds and open to tight, upright folds, respectively, both folding the main foliation with localized development of crenulation cleavages axial planar to the folds. An additional overprint shows no clear cross-cutting relationship with D2 or

GEOSPHERE

GEOSPHERE

https://doi.org/10.1130/GES02742.1

8 figures; 1 table; 2 sets of supplemental files

CORRESPONDENCE: tlpavlis@utep.edu

CITATION: Pavlis, T.L., and Serpa, L.F., 2024, The power of modern 3-D visualization of high-resolution terrain models in geologic mapping: Complex fold geometries revealed by 3-D mapping in the Panamint metamorphic complex, eastern California, USA: Geosphere, https://doi.org/10.1130/GES02742.1.

Science Editor: David E. Fastovsky
Associate Editor: Michael L. Williams

Received 30 November 2023
Revision received 22 January 2024
Accepted 4 March 2024

Published online 25 April 2024

D3 fabrics and could be a manifestation of either of those events, although the

deformation is spatially limited to a narrow shear zone beneath a brittle, dextral-normal fault with the same kinematics as a mylonitic fabric in a Cretaceous granite in the footwall. This observation suggests an extensional, core complex–style deformation to produce this structure. We suggest that

Terry Pavlis https://orcid.org/0000-0002-2993-5438

3-D mapping has the potential to revolutionize geologic mapping studies, particularly where steep topography provides 3-D views that are virtually invisible on conventional 2-D maps. Previously bewildering geologic puzzles can be solved by the ability to visualize large cliff exposures from arbitrary angles and map the features in true 3-D at resolutions to the centimeter level. Although this study emphasized intermediate scales imaged by a drone, our methods here are easily extended to larger scales using a crewed aircraft for imaging. We suggest these methods should be used routinely in frontier areas with steep terrain where aviation is already in use for access, but the methods can be employed anywhere steep terrain "hides" major rock exposures on conventional 2-D maps.

INTRODUCTION

Structure from motion– multiview stereo (SM) photogrammetry (e.g., Westoby et al., 2012; Carrivick et al., 2016) is rapidly becoming a valuable tool for field geology. SM provides three- dimensional (3-D) terrain models that show geologic features at a broad range of scales and orientations with resolution and accuracy to the centimeter to decimeter level (e.g., Pavlis and Serpa, 2023). The models provide an accurate visualization of a site that extends well beyond conventional field observations and can be used for true 3-D mapping with resolution to levels comparable to the model resolution. This ability is particularly transformative in structural geology, where the fundamental observable is documenting geometry yet geometric accuracy is severely limited with conventional field techniques. In complex terranes, SM models allow detailed observations comparable to, or better than, those obtainable in the field and can be revisited using 3-D visualization software as often as needed. This ability can allow unprecedented discoveries when compared to a single- pass, unidirectional visualization during conventional field work. Direct field observations remain important as ground truth, however, because in most cases SM models are limited in their ability to provide all of the traditional field observations. For example, distinguishing similar-appearing rock types, identifying details at hand- specimen or hand- lens scale, and measuring orientations can be difficult to impossible. Nonetheless, SM is extremely useful in providing detailed observations in inaccessible and/or complexly deformed areas at scales at which direct observation is difficult.

SM technology's potential is not limited to structural geology. Geometry is a foundation of many aspects of geoscience. Geomorphologists were some of the first users of SM technology as a natural extension of lidar for terrain models (e.g., Westoby et al., 2012; Colomina and Molina, 2014; Bemis et al., 2014; Brunier et al., 2016). Paleontologists recognized the potential of SM early on with visualization of fossils (e.g., Matthews et al., 2016), and many earth science teachers used SM models of hand specimens (e.g., DePaor, 2016; Andrews et al., 2020) and virtual outcrops (e.g., Cawood and Bond, 2018; Fleming, 2022) during virtual teaching in the COVID-1 9 pandemic. Here we emphasize a structural geology application of SM, but it is important to understand that the applications are potentially much broader. We show an example of how 3-D mapping onto a dense SM point cloud can lead to a new understanding of complex geologic structure. The technology resolved a local structural problem through resolution of geometry and analysis at a variety of scales, an analysis we describe here.

Our example here is from a deep canyon in the Death Valley region of southwestern North America (Fig. 1) where Mesozoic ductile metamorphic structures are exhumed and rock units show significant color contrasts that allow remote recognition of stratigraphic units to aid in resolution of the structure. Thus, the site is a nearly ideal exposure for applications of SM techniques, but comparable results are possible in less- ideal settings. Our SM base model was developed initially from ground- based imagery acquired on the canyon rims (Brush et al., 2018), but new insight was gained from a series of drone flights that allowed higher model resolutions ranging from sub- centimeter to decimeter levels (Pavlis and Serpa, 2023). The scale of our analysis here is larger than those of virtual outcrop models (e.g., Cawood and Bond, 2018) but smaller than those of most traditional geologic mapping projects (tens of kilometers or more) and is focused on that scale because of the nature of the structures observed. Smaller- and larger-s cale analyses can be accomplished with the same technology with the data acquisition method tuned to scale (Pavlis and Serpa, 2023), e.g., smaller areas analyzed as virtual outcrops and larger areas analyzed with imaging from a crewed aircraft (e.g., Svennevig et al., 2015; Rutkofske et al., 2022).

We begin with an overview of the data acquisition and analysis methods employed in

this study, emphasizing the use of high- resolution point clouds as a 3-D mapping base. We then describe the general geology inferred from accessible outcrops in the study area and use these mesoscopic observations together with insights gained by high-r esolution 3-D mapping and remote analysis of orientations on inaccessible cliffs to build an interpretation of the geologic structure. We show in this analysis that all previous interpretations of the geologic structure in this area, including our own, were an oversimplification. Specifically, we present evidence that cliff-f ace exposures exhume sheath folds on the scale of hundreds of meters and that these structures would have been virtually invisible at scales of traditional geologic mapping, particularly on cliff faces like these where the cliffs disappear on a two-d imensional (2-D) map view.

BACKGROUND

Structure-from-Motion–Multiview-Stereo (SM) Technology

SM technology (e.g., Furukawa and Hernandez, 2015; Carrivick et al., 2016) provides an inexpensive method for development of high- resolution terrain models. The method is a generalization of photogrammetric theory where images of any arbitrary orientation are used to simultaneously resolve geometry and camera calibration parameters (Carrivick et al., 2016). The technology is computationally intensive and was impossible prior to development of modern computer systems. Data processing involves two distinct steps (Furukawa and Hernandez, 2015): (1) the “structure from motion” step, where a feature- matching algorithm locates equivalent features within an image set and uses key points on these features to extract (or refine if approximate positions are known) camera positions in space as well as camera calibration parameters, and (2) the “multiview stereo” step where the model is refined by filling in points between key points determined from the structure from motion step. This is a major advancement over conventional vertical incidence photogrammetry that has been used for decades to develop terrain models (e.g., Wolf and Dewitt, 2000) because imaging can be tuned to specific objects of arbitrary geometry by imaging from a wide variety of look directions. For example, steep terrain is always poorly imaged in vertical incidence imagery and is commonly distorted in derivative products like 3-D visualizations derived from orthoimagery (e.g., Pavlis and Mason, 2017; Brush et al., 2018). SM solves that problem, and properly acquired imagery can even provide visualizations of overhanging cliff faces. Because the technique requires imaging of features that can be readily recognized from image to image the method requires constant lighting during image acquisition and a scene with significant contrast, a monotonous gray wall, for example, cannot be imaged. Fortunately, virtually all natural scenes contain objects easily recognized by software, and the technology is very robust for developing high- resolution terrain models.

The relative accuracy of SM terrain models is comparable to that of lidar with absolute positioning depending on the accuracy of the georeferencing methods (Pavlis and Serpa, 2023). As such, this technique is transformative for geologic field studies because a single individual or small team can develop high-r esolution terrain models with minimal effort relative to older technologies like lidar that require fielding heavy equipment that is either ground based or airborne. Instead, in SM a simple camera can be used to acquire images from a variety of look directions either from ground-b ased positions or airborne platforms. Moreover, because the method uses imagery to develop the 3-D model, a point cloud generated for a scene always carries true color information for each point in the cloud (e.g., Pavlis and Mason, 2017). This

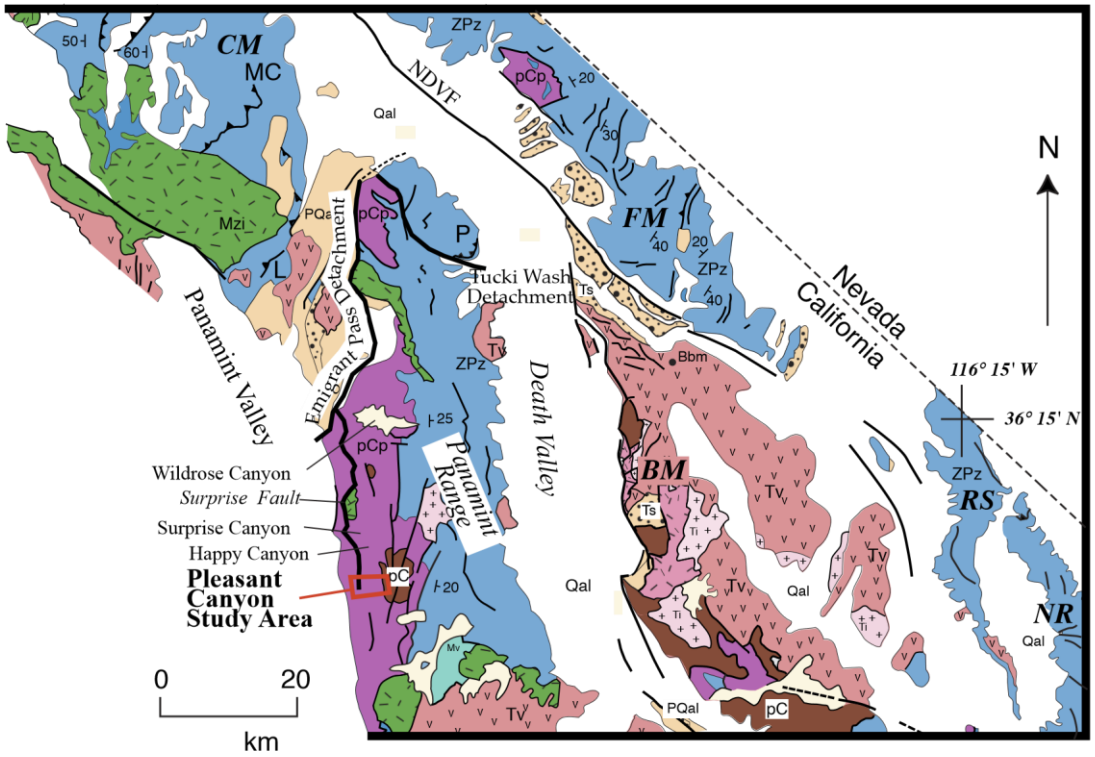

Figure 1. Regional tectonic setting (lower right) and regional geology of study area (main figure), eastern California, USA. Note location of study area in western Panamint Range west of Death Valley. Figure is modified from Miller and Pavlis (2005). Abbreviations: BM—Black Mountains; CM—Cottonwood Mountains; FM—Funeral Mountains; L—Lamone thrust; MC—Marble Canyon thrust; NDVF—Northern Death Valley fault; NR—Nopah Range; P—

Cenozoic Igneous rocks

Tv

Ti

Mv

Sediments, Sedimentary Rocks

Qal

PQal

ZPz

pCp

pC

Panamint thrust; RS—Resting Volcanic rocks, and Metasedimentary Rocks **Spring**

Range; SAF—San Anmostly late Tertiary**dreas fault; MX—Mexico.**

Quaternary

alluvium

Neogene intrusive rocks

undifferentiatedPliocene-

Ts

Quaternary deposits

I-20

Strike and dip of

sedimentary bedding

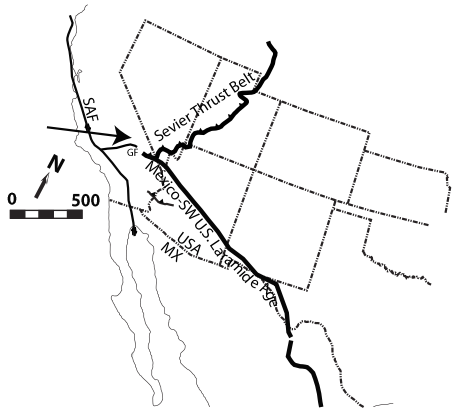

ary sedimentary rocks

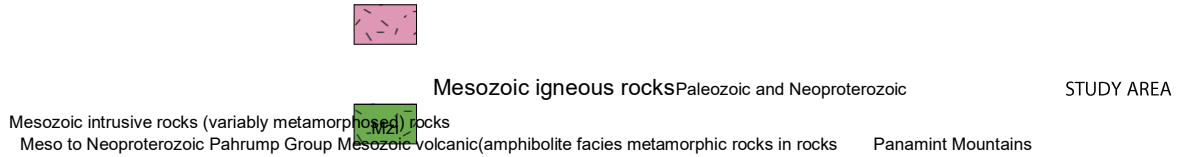

feature is a critical element of SM because each point in the point cloud is essentially a 3-D color pixel and a visualization of a SM point cloud always shows true colors in their proper position in 3-D space (Pavlis and Serpa, 2023).

Visualization of 3-D terrain models has traditionally emphasized mesh visualizations (e.g., V3Geo and the software package LIME; https:// www .virtualoutcrop .com /news /V3GeoLaunch). Mesh visualizations are developed by using a point cloud to generate a triangular mesh surface with imagery projected onto mesh elements, producing a visualization with resolution comparable to that of the camera. Mesh visualizations are essential for visualizing terrain with a low- resolution elevation model like a digital elevation model (DEM; e.g., Google Earth) or a sparse lidar point cloud. With SM data, this approach is questionable for developing a 3-D base for geologic mapping. We prefer point cloud visualizations over mesh visualizations in SM data because data quality can be readily observed on the point cloud but may be masked in mesh visualizations, e.g., sparse data are obvious on a point cloud but are commonly invisible on mesh models. This feature contrasts with the characteristics of lidar, which commonly is acquired with no imagery, and colorizing the scene to produce a 3-D visualization requires an image drape that is subject to registration errors (Pavlis and Serpa, 2023). In areas of low relief, this distinction between lidar and SM data may not be significant, but in areas of steep terrain, image drape errors can be large and nearly invisible in the absence of other data (e.g., Brush et al., 2018).

Most SM models have been developed at what we refer to as virtual outcrop scales or scenes from <1 m to a few tens of meters across (e.g., McCaffrey et al., 2008; Tavani et al., 2014; Wilkinson et al., 2016; Cawood and Bond, 2018). Although visualizations at these scales are powerful aids to show geologic features, particularly as teaching tools (e.g., Cawood and Bond, 2018; Andrews et al., 2020; Fleming, 2022), the gains from these types of visualizations are, in our opinion, relatively incremental because this is the scale range of traditional field observations. Specifically, in any field study, individual outcrops are examined by looking at the exposure from various angles and scales. This is the approach most geologists use in unraveling the meaning of a specific exposure and is also the power of 3-D outcrop visualizations, i.e., the ability to visualize the feature from different directions and at different scales. The only distinction in 3-D visualizations is that the task can be done at a computer screen rather than walking around the exposure. This is not the case for larger exposures at what has traditionally been called “macroscopic scale” in structural geology (e.g., Davis et al., 2011).

Macroscopic-s cale structural problems have traditionally been solved using a map-based approach. In this approach, outcrop observations are recorded as points on the map base with critical data synopsized as symbology (e.g., orientation symbols), and linework is drawn on the map to delineate rock units or structural features (e.g., structural objects like axial traces of folds or form lines of foliation traces). In the early 21st century, this approach evolved into modern digital mapping techniques that first used GIS- based systems (e.g., Walker and Black, 2000; Pavlis et al., 2010) and are now evolving to more advanced systems like StraboSpot (https://strabospot.org/; Walker et al., 2019).

Map- based macroscopic analysis works very well where topographic relief is modest and

where exposure is poor to moderate. In areas where exposure is extensive, particularly in steep terrain with near- vertical cliffs, the map- based structural analysis method often fails because the same areas that carry the most information, the cliff faces, are virtually invisible in a map view. In the past, this limitation of map representations was typically accommodated by ad hoc methods ranging from field sketches of cliff faces to photographic panoramas of exposures. SM solves this problem. A SM model of a cliff face can provide a true 3-D visualization of the surface, and mapping features onto that model, a direct extension of the traditional macroscopic mapping method, is a major step forward in understanding geometry at macroscopic scale. Here we present an example of the power of this approach.

Geologic Setting of the Study Area

The area of this study is the Panamint Range in the Death Valley region of southwestern North America (Fig. 1). The area lies within the southern North American Cordillera, where there have been persistent 3-D complexities that extend through a large swath of geologic time. We emphasize the 3-D complexities here because regional geology suggests 3-D kinematics over time that presumably is reflected in the rock record of the Panamint Range. The record is further complicated by high finite strains which influence local interpretations (see details in Macroscopic Structure in Pleasant Canyon section).

The main history of the area began in the late Proterozoic with the development of the Cordilleran passive margin and deposition of the miogeoclinal stratigraphy onto Mesoproterozoic basement. Following deposition, the assemblage was subject to a series of deformational events, most of which deviated from simple coaxial deformation over time.

In the late Paleozoic to early Mesozoic, the passive margin was truncated by sinistral strike slip and subsequent nucleation of a NE-d ipping early Mesozoic subduction zone that produced a magmatic arc across the truncated passive margin (e.g., Walker, 1988; Busby- Spera, 1988; Stevens et al., 1992). Magmatic activity in this arc initiated metamorphism of the rocks in the study area (e.g., Labotka et al., 1985) with associated deformation generally linked to back- arc contraction. By the mid- Mesozoic, the area lay in the hinterland of the Sevier orogenic belt, a well-k nown back- arc contractional belt that has been documented for decades (e.g., Burchfiel and Davis, 1972) and remains the subject of study (e.g., DeCelles, 2004; DeCelles and Graham, 2015; Yonkee and Weil, 2015). At this latitude, contraction directions in the Sevier belt vary along strike and are complicated by Neogene extension and transtension. To the north and east, thrust systems were ESE to SE directed (e.g., Yonkee and Weil, 2015), but just to the south and east, in the Mohave Desert region, structural trends take a nearly 90° bend due to both paleogeography and younger deformation. In particular, to the east (Fig. 1), the orogen merges with the Mexican segment of the orogen where contraction is generally younger (Late
Cretaceous and Paleogene) and overlaps in time with the “Laramide orogeny” characterized by foreland deformation in southwestern North America (e.g., Busby et al., 2023).

The study area lies in the transition zone between these major orogenic trends, with the rock record to the east of the Panamint Range distinct from that to the west. To the east, early studies inferred little, if any, Laramide-a ge deformation in the region with Jura-Cretaceous thrust systems showing E- to ESE-d irected transport (e.g., Burchfiel et al., 1992). More recent studies (e.g., Pavlis et al., 2014; Lima et al., 2018), however, suggest Laramide-a ge overprints may be significant. Specifically, Pavlis et al. (2014) showed evidence from the Nopah and Resting Spring Ranges (Fig. 1) that two kinematically distinct contractional events affected that area: an older, Jura- Cretaceous event kinematically and temporally linked to ESE- directed thrust systems of the Sevier belt, and a younger, latest Cretaceous– Paleogene (Laramide age) event with NE-d irected contraction. To the west of the Panamint Range, however, Laramide-a ge deformation is cryptic to absent and an older series of structures is well documented (e.g., Stevens and Stone, 2005; Stevens et al., 2015). Specifically, back- arc contractional structures of the Sevier belt merge with structures generated during a complex late Paleozoic to present- day history that includes (Stevens and Stone, 2005; Stevens et al., 2015): (1) relatively cryptic structure inherited from the late Paleozoic to early Mesozoic sinistral strike slip that truncated the passive margin (Stevens et al., 1992); (2) Permo- Triassic contraction commonly linked to Cordillera-w ide collapse of a marginal basin system (e.g., “Sonoman orogeny” and associated Golconda allochthon recognized in Nevada) that includes somewhat older structures in this region (e.g., Stevens et al., 2015); (3) E- to ESE-d irected thrust systems assumed to be part of the Sevier belt; (4) Jurassic NE-d irected thrust systems of the Eastern Sierran thrust system (e.g., Dunne and Walker, 2004); and (5) mid- Cretaceous dextral strike- slip systems in the Sierra Nevada (e.g., Tikoff and de Saint Blanquat, 1997; Trevino and Tikoff, 2023) as well as Neogene strike-s lip systems linked to Neogene extension.

Given the location of the Panamint Range between these two distinct structural provinces, it should be no surprise that the structure of the Panamint Range is complex. Here we describe some of that complexity and attempt to unravel structural geometries that bear on this history. Full resolution of that history requires a clear resolution of the absolute ages of structures as well as a more regional approach than we use here and is the subject of ongoing work to be reported elsewhere.

REGIONAL GEOLOGIC RELATIONSHIPS IN THE PANAMINT RANGE

The northern Panamint Range (Fig. 1) is the subject of extensive studies in the 1980s that focused on detachment fault systems at Tucki Mountain (e.g., Hodges et al., 1987, 1990; Wernicke et al., 1988, 1989, 1993). Those studies demonstrated that two major detachment systems cut the assemblage.

The structurally lowest detachment is the Tucki Wash fault system, which separates

unmetamorphosed rocks from underlying metasedimentary rocks (Fig. 1), preserving a supracrustal thrust in the hanging wall and a ductile thrust below (Wernicke et al., 1993). The aforementioned studies correlated the Panamint thrust in the hanging wall with the ductile footwall thrust system, which implies that rocks in central Panamint Range lay in the hanging wall of that thrust system. The Tucki Wash detachment and thrusts it cuts are in turn cut by a younger, structurally higher-l evel detachment, the Emigrant Pass detachment, which carries a Neogene sedimentary basin in its hanging wall (Burchfiel et al., 1987; Hodges et al., 1989; Snyder and Hodges, 2000) and cuts obliquely through the northern third of the Panamint Range (Fig. 1). The Emigrant Pass fault was deactivated when oblique-s lip faults formed along the modern western escarpment of the Panamint Range, exhuming the syn- extensional Nova Basin (Burchfiel et al., 1987; Hodges et al., 1989).

The Emigrant Pass low- angle normal fault system merges with the active mountain front of Panamint Valley near Wildrose Canyon (Fig. 1). The Nova Basin stratigraphic assemblage disappears near Wildrose Canyon, but a distinct low-a ngle fault continues to the south carrying a series of brecciated older rocks in its hanging wall. Andrew (2022a) correlated this fault to the Emigrant Pass detachment fault. In their compilation map, however, Workman et al.
(2002) distinguished this structure from the Emigrant Pass detachment as the Surprise fault, presumably because Albee et al. (1981) mapped the hanging- wall assemblage as brecciated older rocks rather than basinal sediments. From upper Wildrose Canyon to just south of Happy Canyon (Fig. 1), isolated klippen of a low-a ngle fault that is presumably part of this low-angle normal fault sys tem has been mapped (Albee et al., 1981; Harding, 1987; Hodges et al., 1990; Andrew, 2002, 2022a). These klippen exemplify the east tilt of the range block with fault dips on the klippen of <10°. In the central Panamint Range, however, slip on this fault system is not large given that metamorphic grade does not change significantly across the fault(s) and in most cases there are footwall cutoffs recognizable up dip on the fault system. Below this nearly flat- lying fault system, the metamorphic assemblage is essentially an intact crustal slice with only minor faults apparent (e.g., Albee et al., 1981; Andrew, 2022a, 2022b; this study). This general observation is important because it implies the central Panamint Range can be restored to pre-e xtensional geometry by a simple rigid- body rotation of 30°–60° to the west to restore both the dip of cover to the east and the faults to a likely original west dip of >30°. This assumption is further justified by low- temperature thermochronology data from the central Panamint Range (Bidgoli et al., 2015) that show preservation of Paleogene cooling ages that young to Neogene ages to the west, consistent with simple exhumation of a crustal slice.

Below the low- angle normal faults in the central Panamint Range, the rocks become successively higher- grade metamorphic rocks from east to west (Labotka et al., 1980; Labotka, 1981), coincident with the decrease in cooling ages recognized by Bidgoli et al. (2015). The metamorphic rocks are primarily metasedimentary rocks that have been correlated to the Pahrump Group (Fig. 2) and overlying Neoproterozoic section as well as local exposures of gneissic rocks that are interpreted as Precambrian basement (Albee et al., 1981).

METHODS

The focus of this study was on the development of 3-D mapping techniques in complexly deformed metamorphic terranes. Brush et al. (2018) and Pavlis and Serpa (2023) describe the approaches used in this study and limitations of the methods, but we reiterate some of these methods to emphasize the accuracy of the mapping we report here. In this paper, we refer to 2-D, 2.5-D , and 3-D mapping, which have specific meanings that are relevant to our results:
(1) 2-D (two-d imensional) mapping refers to conventional mapping on a flat- map base where all data are projected, or mapped directly, to this 2-D surface; (2) 2.5- D mapping refers to mapping on a 3-D rendering of terrain but where imagery, 2-D base maps, and other data layers are draped onto the terrain model by projection along the *z* (vertical) axis—a method requiring orthocorrection of imagery draped onto the terrain model; and (3) 3-D mapping refers to mapping on a terrain model that is a full- color, accurate 3-D rendering of the scene, free from distortions or mislocation of objects in the scene—i.e., objects are in their proper position in 3-D space and are their proper shape and size for viewing from arbitrary look directions.

In this study, we began with conventional 2-D geologic mapping on an orthophoto base co- referenced to a topographic map using a digital mapping approach similar to that described by Pavlis et al. (2010) with the variant that we used the open- source GIS program QGIS. These data are compiled in Item S1 of the Supplemental Material[1] together with mapping corrected through true 3D mapping. The data structure is similar to that of Pavlis et al.'s (2010)

[1] Supplemental Material. Item S1: GIS files used to construction Figure 4. Item S2: Three animation files showing the SM terrain models (Items S2a and S2b showing north and south canyon wall respectively) and animation of the interpretation (Item S2c) without the background model. Item S3: 3- D PDF files of the SM terrain models; north and south walls of the canyon are in separate files. Please visit https://doi.org/10.1130/GEOS.S.25511392 to access the supplemental material, and contact editing@geosociety.org with any questions.

Johnnie Formation

Upper Noonday (N3) (Mahogany Flats Member) upper Radcliff Member
lower Radcliff Member
Sentinel Peak Member

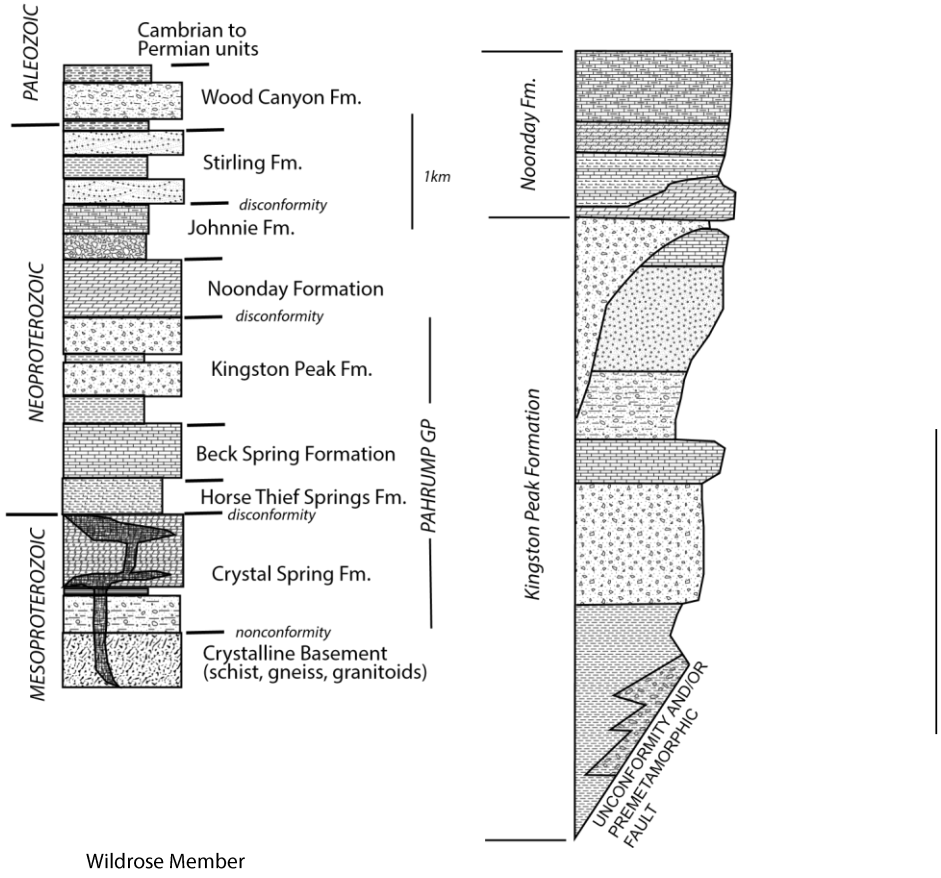

Wildrose Member

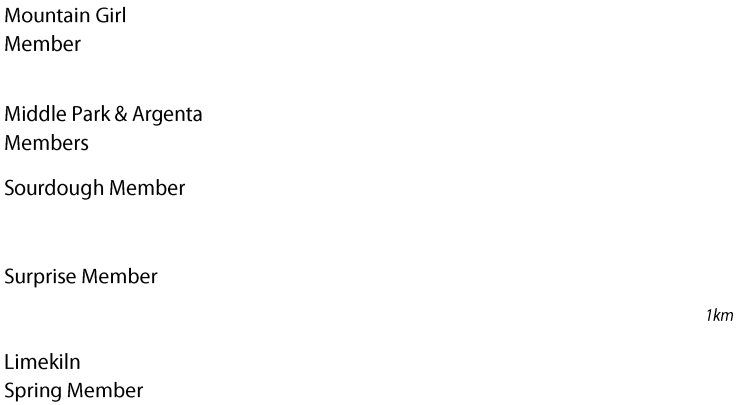

Figure 2. Generalized stratigraphic section for the study areas. Established Proterozoic to earliest Cambrian stratigraphic units (left) are after Levy and Christie- Blick (1991), Burchfiel et al. (1983), and Mahon et al. (2014). Figure on right is enlargement of main stratigraphic units established as members of Kingston Peak and Noonday Formations with our mapping generally following these divisions (modified from Petterson et al., 2011). Note scale showing stratigraphic thicknesses for Noonday and Kingston Peak are only generalities because all units show extreme variations due to both primary sedimentary depositional variation and finite strain related to syn- metamorphic flow. See text for discussion of these issues.

Figure 3. Field photographs of mesoscopic structures in western Panamint Range. (A, B) LS tectonite fabric marked by deformed objects (conglomerate clasts) in Mountain Girl Member of Kingston Peak Formation. Both images are from exposures in Pleasant Canyon, with A showing very high strains measured at 13tpp10 (see Figure 5 for location and text for details) and B showing more modest, constrictional strains (view shows foliation surface and a plane approximately perpendicular to lineation) away from the high-strain zone. A and B are approximately the same scale with the geoclino electronic compass device ~18 cm long. (C) Deformed objects (rip-up clasts) in *XZ* (parallel to lineation, perpendicular to foliation) section of marbles derived from Radcliff Member of Noonday Formation in upper Wildrose Canyon. Image implies large finite strains, although actual strain magnitudes are difficult to measure due to initial depositional fabric of rip-up clasts. (D, E) Original (D) and annotated (E) images showing transposed layering due to isoclinal folding in Radcliff Member marbles in upper Wildrose Canyon. View is approximately perpendicular to fold axes (view to north). Note that finite strains in Wildrose Canyon are likely far lower than in comparable rocks in Pleasant Canyon. Scale in D and E is indicated by tip of a walking pole. (F) Outcrop of interbedded greywacke and shale from Lime Kilmkiln Springs Member of Kingston Peak Formation deformed into isoclinal folds, with main foliation axial planar to folds (annotations show layering as blue and foliation orange). Image is from lower Surprise Canyon. Image view is ~10 m across. (G) Development of F3 mesoscopic folds and S3 crenulation cleavage overprinting main foliation in Wildrose Canyon (annotations in purple show axial surfaces and S3 traces). Image view is ~3 m across. (H) View toward north (perpendicular to fold axes) of mesoscopic type 1 and type 2 interference patterns in folded layering in marbles derived from Thorndike Member of Kingston Peak Formation in Pleasant Canyon; patterns result from either superposition or sheath folding (see text for discussion). Black lines are annotations showing outlining traces of layering on the exposure. View is ~2 m across.

metamorphic project. This mapping was conducted over four short field seasons in three field focus sites (Wildrose, Surprise, and Pleasant Canyons; Fig. 1) with results from the Pleasant Canyon site reported here. These methods, however, proved inadequate for resolving the structure in the focus sites because the sites were in steep- walled canyons with very limited access and cliffs that were invisible on the traditional 2-D map base. Thus, these field studies were primarily devoted to establishing outcrop-s cale structural relationships and relative chronologies, i.e., mesoscopic structural analysis in traditional terminology (e.g., Davis et al., 2011; Fig. 3). These traditional field techniques are the basis for the mesoscopic descriptions in this paper.

During spring 2014 field work, we also conducted a terrestrial lidar survey (TLS) in parts of the three study areas using UNAVCO (Boulder, Colorado, USA) equipment and assistance from a UNAVCO technician with the objective of experimenting with these data as a 3-D mapping base. The TLS data were processed at UNAVCO, and we used the processed data as initial background data for 3-D mapping. During the 2014 field season, however, we also acquired a series of ground- based photographs that were used to develop SM- based terrain models from the imagery using Agisoft PhotoScan software. Based on those initial results, we realized SM was potentially transformative and ultimately used the TLS primarily as a georeference source for the SM models and did our geologic interpretations on SM point clouds (e.g., Brush, 2015; Pavlis and Mason, 2017; Brush et al., 2018; Pavlis and Serpa, 2023).

Based on analysis of the ground- based SM models (Brush et al., 2018), we revisited a site in Pleasant Canyon that appeared to contain exposures with potential to unravel structural details, and analysis of data from this site is the focus of this paper. Specifically, we used a DJI Mavic 2 Pro drone to image what Brush et al. (2018) referred to as the Noonday structure in a series of manual imaging and autonomous flights that provide unprecedented detail of the structural geometry on the cliff faces of the canyon (see Pavlis and Serpa,
2023, for details on data acquisition). The drone was equipped with an onboard GPS system with real- time differential positioning that provided 3-D camera positions. Thus, placement of ground control points was not necessary, and models were referenced exclusively through camera positions (see Pavlis and Serpa, 2023, for assessment of the accuracy of this method). The drone imagery was processed in Agisoft Metashape and Pix4D software and evaluated for accuracy relative to the lidar terrain model using CloudCompare software (Pavlis and Serpa, 2023). Analysis of the data revealed that the drone- based models we use here have a resolution of 5–7 cm, and when registered to the TLS data, have an accuracy comparable to the 3–5 cm accuracy of the lidar base (Pavlis and Serpa, 2023).

After terrain models were generated, we registered all the data to the lidar data using utilities in Maptek PointStudio software and mapped directly onto the point clouds using CAD utilities in PointStudio. Animations (File S2) and 3-D PDF files (File S3) were generated in PointStudio. Note that without the TLS base, the individual data sets from different flights and ground- based imaging would have potential registration errors of a few meters, with error in line with that of conventional differential GPS or errors from use of natural objects for georeference (Pavlis and Serpa, 2023). Although potentially problematic for areas lacking a lidar reference model, we have found that if individual surveys overlap 30% or more, a series of surveys can be merged into a coherent, single reference frame by choosing a centrally located model for reference and registering adjacent models to the reference model using utilities in either PointStudio or CloudCompare. Further research is needed on how far this approach can be extended, but for this study, we were able to register all of the SM data to the TLS data to within ~1 m.

During mapping, we developed a procedure of tracing linework onto the model then selecting linework for individual objects and viewing them in 3-D to evaluate geometry. This method allowed recognition of mapping errors, and we used the method to iteratively redraw lines across covered intervals or areas where lithologic contacts were hard to follow on the scene. After completing the mapping, we exported the linework to QGIS where we used the linework to develop the map- view representation of the rock units (Fig. 4) and two cross sections using the plugin qProf. Ground truth for these remotely sensed interpretations was obtained from previous traverses on the ridgetops above the canyon walls and limited observations on the lower slopes.

The high resolution of the mapping in true 3-D allowed construction of cross sections (Fig. 5) with virtually no interpretation beyond the interpretations of the map itself. That is, 3-D linework projected to the sections along fold trends produced a nearly perfect rendering of the sectional geometry with the only artifacts arising from structure that was not 2-D (e.g., curved fold axes), projection of lines well off section beyond reasonable projection distances, or both. This observation is consistent with conclusions of Pavlis and Serpa (2023) that the models have relative accuracies to submeter levels.

Finally, we evaluated remote orientation measurement methods on cliff faces using point picking on the 3-D models. Both CloudCompare and PointStudio have utilities for multipoint measurements to obtain a planar best fit to the point data set. This method is

essentially the multipoint equivalent of the three- point problem taught in virtually all undergraduate structural geology courses. Specifically, the user finds a feature that appears to be planar and picks a series of points on the feature, and the program calculates a best-fi t plane to the data. In this study, we used PointStudio because the tool is easier to use than the CloudCompare plugin and generates a visualization disk to easily evaluate the accuracy of the measurement.

GEOLOGY OF THE CENTRAL PANAMINT RANGE

Stratigraphy

All the rocks in the western Panamint Range were metamorphosed at low- pressure, upper greenschist to amphibolite facies (Labotka, 1981) with protoliths derived primarily from sedimentary cover but also fully involving Mesoproterozoic basement rocks. Albee et al. (1981) recognized that the metasedimentary rocks were derived primarily from the Pahrump Group and

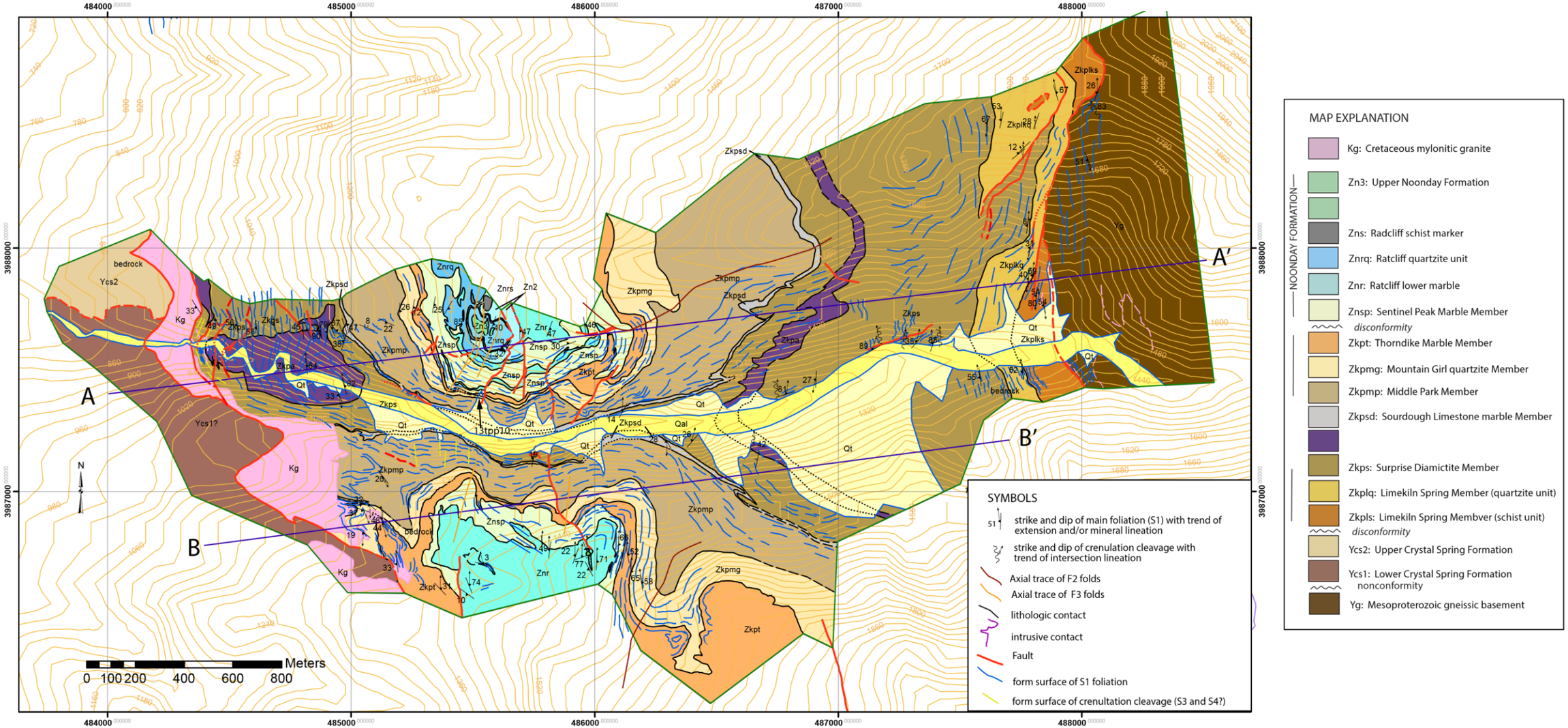

Figure 4. Conventional geologic map (A) and map explanation (B) of study area. Cross sections shown in Figure 5 are marked.

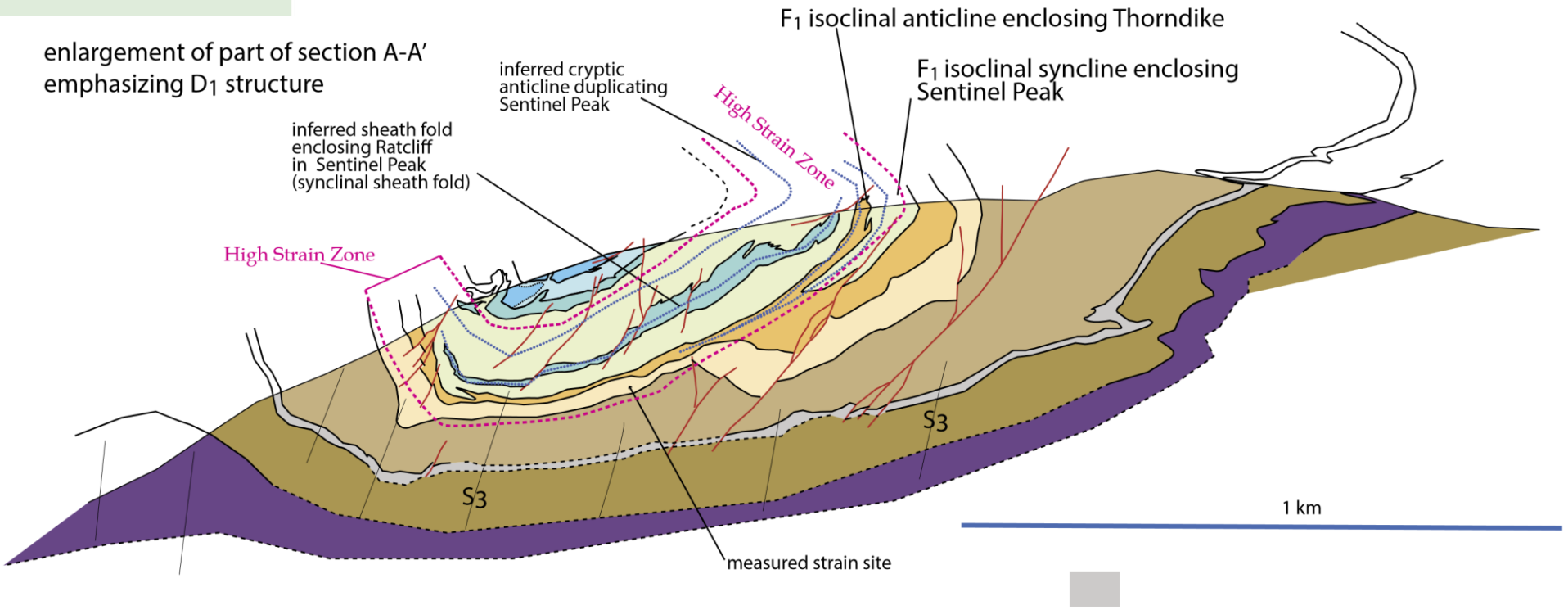

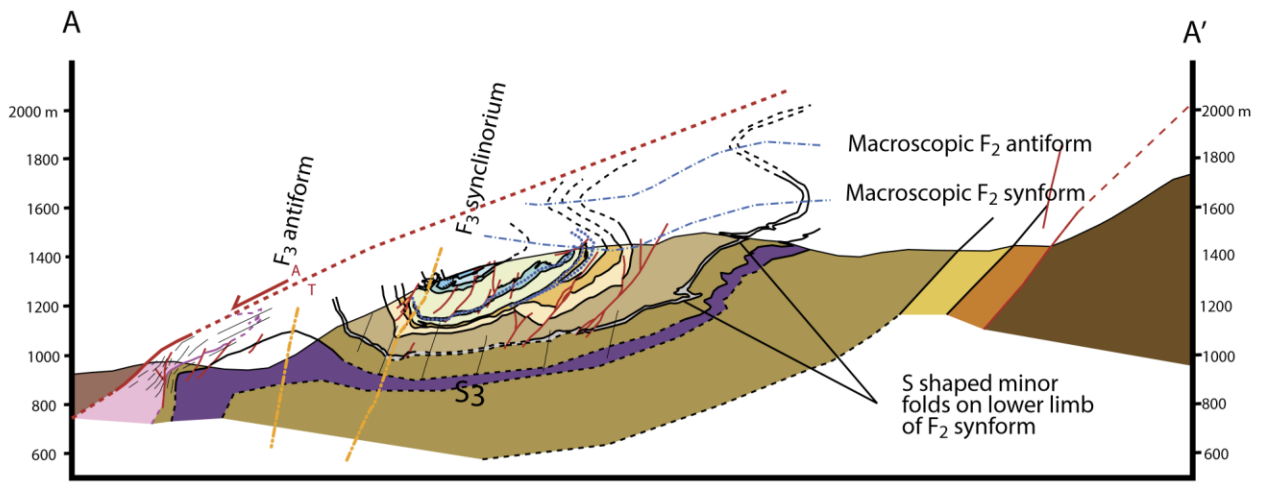

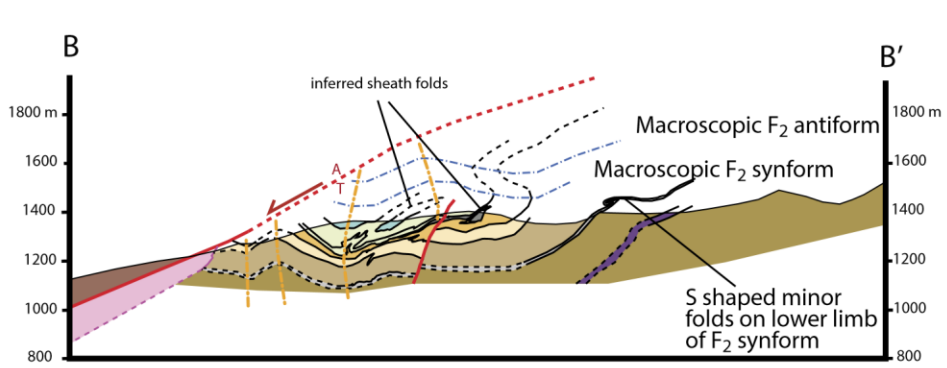

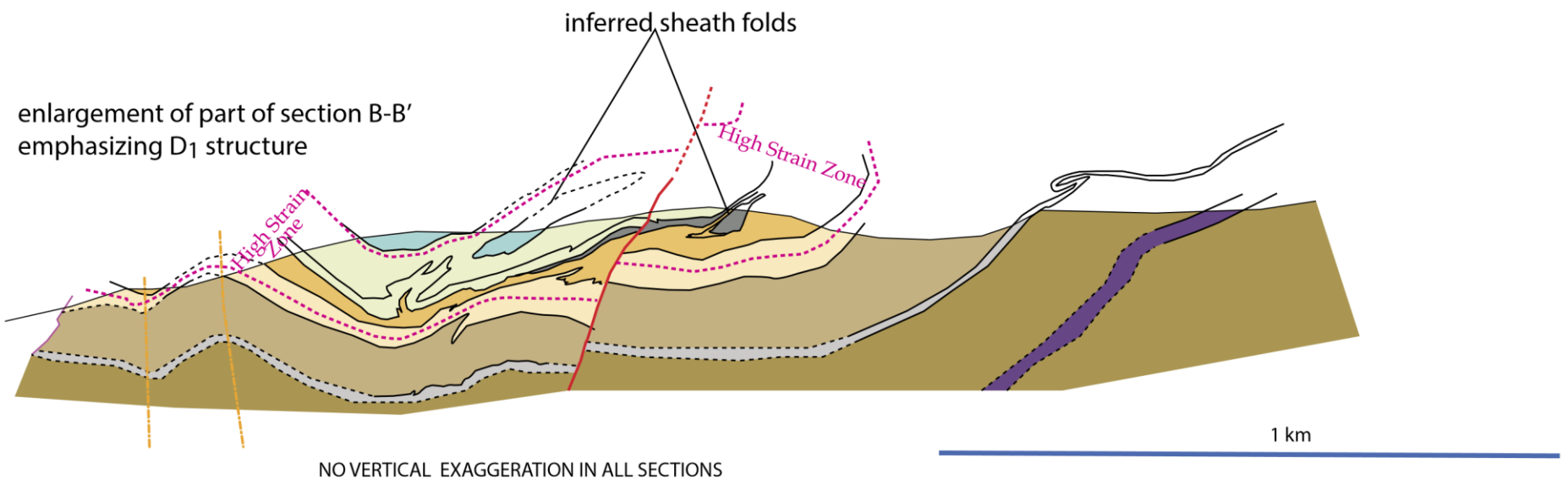

NO VERTICAL EXAGGERATION IN ALL SECTIONS

Figure 5. Cross sections A-A′ and B-B′ shown in Figure 4 with enlargements of major structural features mapped in three dimensions.

overlying Neoproterozoic rocks (Fig. 2). These Proterozoic sedimentary rocks are well described to the east where weakly metamorphosed equivalents are well exposed in the southern Death Valley region. Mrofka and Kennedy (2011), Petterson et al. (2011), Macdonald et al. (2013), and Nelson et al. (2020) summarized this correlation and emphasized similarities and distinctions between the sections in the Panamint Range and southern Death Valley. Our studies support the evolving view that the Neoproterozoic stratigraphy contains major lateral facies changes related to deposition in a syn- rift environment (e.g., Nelson et al., 2020), but we also show here that structural complexities handicap full interpretation of the stratigraphic history until the structure is fully understood.

Figure 2 summarizes the primary stratigraphic units recognized in the western Panamint Range, but a one- dimensional stratigraphic column simplifies a section with numerous unconformities and lateral facies changes. In this study, several observations are important to geologic mapping presented in Figures 4 and 5:

(1) Proterozoic basement and the directly overlying Crystal Spring Formation, Horse Thief Springs Formation, and Beck Springs Formation represent a readily recognizable stratigraphic sequence. Regional studies (e.g., Wright et al., 1976) support the concept these units represent a pre-r ift stratigraphy that has significant lateral continuity such that subunits can be recognized over large areas, except where unconformities cut out the section.

(2) The lower Pahrump Group section (Fig. 2) is overlain by the syn-r ift Kingston Peak Formation, which is characterized by significant lateral facies variations (e.g., Nelson et al., 2020). These lateral facies variations complicate regional mapping but are insignificant at the scale of Pleasant Canyon, with all the units fitting into established stratigraphy.

(3) The Kingston Peak Formation is unconformably overlain by the Noonday Formation (Fig. 2). The Noonday shows lateral facies variations similar to those of the underlying Kingston Peak reflecting continuation of syn- rift sedimentation, but the unit is composed primarily of carbonate rocks reflecting the end of glacial conditions (e.g., Macdonald et al., 2013). Petterson et al. (2011) proposed a redefinition of the unit over the Death Valley region using subdivisions developed in the Panamint Range, and we follow those subdivisions here (Fig. 2) with some caveats.

Mesoscopic Structure

Throughout the western Panamint Range (Fig. 1), we recognize a similar structural history recorded as fold systems and fabric overprints. Our observations indicate more complex structure in this region than earlier studies by Albee et al. (1981) and Labotka et al. (1980) but are consistent with descriptions in the northern Panamint Range by Hodges et al. (1987) and the southern Panamint Range by Andrew (2002, 2022a, 2022b).

At mesoscopic scales, all pre– late Mesozoic rocks in the west- central Panamint Range

are metamorphic tectonites that display a pronounced continuous cleavage (S1). The principal fabric is an LS fabric in which fabric axes are demonstrably parallel to finite strain axes based on numerous finite strain markers in metaconglomerates and diamictites (Figs. 3A and 3B). The foliation (S1) is generally parallel to layering (S0) and defined by both object shapes and crystallographic preferred orientations of micas, amphiboles, or both. The lineation is formed by elongate minerals (L_m), elongate objects—primarily pebbles in metaconglomerates and diamictites (L_{ext})—or both, with the elongate objects demonstrating the lineation is a stretching lineation (Figs. 3A and 3B). In marbles, this main fabric is inconspicuous due to recrystallization, with the planar fabric defined by layering transposed by isoclinal folding (Figs. 3C–3 E). In contrast, metamorphosed diamictites typically display only a finite strain fabric and crystallographic fabrics because the protolith lacked primary sedimentary bedding. In layered rocks, particularly metapelites (Fig. 3F), S1 is axial planar to numerous mesoscopic close to isoclinal folds (F1) with axes parallel to the main lineation (L_m and L_{ext}). Thus, the lineation is a composite lineation representing both a stretching axis and an intersection lineation. In marbles where recrystallization has obliterated crystallographic fabrics, a lineation is still commonly present in fold hinge zones, primarily because of preservation of the intersection lineation component in the fabric.

S1 is conspicuously folded on mesoscopic to macroscopic scales with folds of two distinct orientations: (1) a ubiquitous group of horizontal to gently plunging, upright to steeply inclined, open to close folds (Fig. 3G) and (2) localized macroscopic folds that are horizontal to gently plunging, recumbent to gently inclined, tight to sub- isoclinal folds (Figs. 3– 5). Schists and some amphibolites contain a prominent crenulation cleavage that is axial planar to the upright folds in foliation (Fig. 3G), but that cleavage is conspicuous only in the hinge zone of folds and generally is limited to schists where the pre- existing mica foliation shows the overprint. The recumbent folds also display a localized crenulation cleavage in the hinge zones of folds, but this overprint is not prominent on fold limbs. Based on differences in fold style and macroscopic relationships described in the next section, we interpret the recumbent folds as a second- generation fold system (F2) and the upright folds as a younger generation (F3).

Like Hodges et al. (1987) at Tucki Mountain (Fig. 1), we observe scattered evidence of an earlier folding event, F1a, that predates the main continuous cleavage. This fold system is prominent at outcrop scale where interference patterns in layering suggest refolded fold patterns, isolated fold hinges, or both. Using the terminology of Ramsay (1967), interference patterns associated with this F1- F1a overprint are typically type 3 reflecting coaxial folding, but type 2 and type 1 patterns (Fig. 3H) are also observed, particularly in the middle (Radcliff) member of the Noonday Formation. Conversely, however, these apparent interference patterns may reflect sheath folding, a hypothesis we consider here.

Macroscopic Structure in Pleasant Canyon

Pleasant Canyon affords the best illustration of the complexity of metamorphic structures in the Panamint Range through direct visualization of the canyon walls where cliff exposures and strong color contrasts between rock units allow interpretation of structures (Items S2 and S3, see footnote 1). Brush (2015) and Brush et al. (2018) described this area using 3-D models derived from ground-b ased imaging, but our new, higher-resolution data and improved images of the south canyon wall provide new insight. Our mapping (Fig. 4) covers only a subsection of the assemblage but provides the first clear picture of the structure with the primary insight gained by 3-D mapping on the SM point clouds (Files S2 and S3). We describe the structure from east to west, which is from structurally highest to lowest level due to range tilt but also from stratigraphically deepest to highest level because of complex structure. We use the 2-D geologic map reference (Fig. 4) for the basic description, but 3-D views (Figs. 6 and 7; Files S2 and S3) are critical for illustration of structural details.

The eastern limit of our mapping includes extensive exposure of Proterozoic crystalline basement (Fig. 4) in a D3 structural high that Labotka et al. (1980) referred to as the World Beater dome. The main fabric in the basement assemblage is probably Mesozoic given that it is subparallel to fabrics in overlying cover. Nonetheless, this conclusion is tentative because four different mapping efforts (Albee et al., 1981; Cichanski, 1995; Andrew, 2022a; this study) disagree markedly on the nature of the basement-c over contact in this area. Albee et al. (1981) and Cichanski (1995) showed the contact as a nonconformity with the Limekiln Spring Member of the Kingston Peak Formation on basement. Andrew

(2022a) showed an erosional remnant of the lower Crystal Springs Formation on

basement unconformably overlain by Limekiln Spring Member rocks. Although this contact was not a focus of our study, stratigraphic relationships have regional implications (e.g., Wright and Troxel, 1967). Our observations suggest a third alternative, that the basement-c over contact is a fault in the mapped area. Evidence for a fault includes low-angle cutoffs of lithologic units in cover against the contact (Fig. 4A), fault rocks along the contact, and a hydrothermal halo demonstrated by mineral exploration and production pits that follow the contact. In addition, recent stratigraphic work by Nelson et al. (2020) measured an intact section across the basement-c over contact in lower-grade rocks just to the east where the basal Kingston Peak unconformity cuts out all older rock units. The lower half of their basal unit is missing in lower Pleasant Canyon, consistent with a fault contact cutting out that unit. Andrew's (2022a) mapping of the lower Crystal Springs Formation is allowable from our limited mapping because we may have misidentified the lower Crystal Springs given that the metamorphosed quartzofeldspathic sedimentary rocks of the lower Crystal Springs can be hard to distinguish from quartzofeldspathic basement rocks. Nonetheless, the evidence for a fault contact seems clear.

The presence of a fault contact is important because aside from the basal unit of the assemblage, the Limekiln Springs Member of Albee et al. (1981), the Kingston Peak Formation stratigraphic units recognized by Labotka et al. (1980), Prave (1999), and Nelson et al. (2020) that are recognizable through the Panamint Range can be mapped in lower Pleasant Canyon, albeit with structural complexity (Fig. 4). The uppermost Kingston Peak unit, the Wildrose diamictite member, is not prominent in the mapped area, limited to thin horizons tentatively mapped on cliff faces but unconfirmed by direct observation (Figs. 6 and 7).

In the mapped area (Fig. 4), the most prominent structure is an open to tight, upright synform with a half wavelength of ~3–4 km (Fig. 5). This structure is the only fold mapped in Pleasant Canyon by Albee et al. (1981) and Cichanski (1995), and in detail the structure is a synclinorium comprising a synform-a ntiform-synform triplet that varies in style along trend (Fig. 5). In our relative chronology (Table 1), this synclinorium is an F3 fold because it folds older foliations and is associated with a steeply dipping crenulation cleavage

TABLE 1. OBSERVED DEFORMATION SEQUENCE

Deformation event	S (planar fabric)	L (linear fabric)	F (folds)	Orientation	Note
D4?	Mylonitic foliation and crenulation cleavage	Stretching lineation	Microfolds in metasedimentary rocks	Gently to moderately W-dipping foliation, NW-trending lineation	Mylonitic fabric in granite extends into adjacent metasediments as crenulation cleavage; generation uncertain
D3	S3 domainal crenulation cleavage	L3 crenulation intersection lineation on S1	F3 meso- to macroscopic, open to tight, upright horizontal folds in S1 foliation	S3 N-NNW striking and steeply dipping, horizontal to gently plunging folds and intersection lineation	F3 folds all older fabrics and Cretaceous dikes; macroscopic folds documented for decades
D2	S2 domainal crenulation cleavage	L2 crenulation intersection on S1	F2 localized recumbent to gently inclined tight to close folds in S1 foliation	S2 and F2 axial planes subhorizontal, F2 axes horizontal to gently plunging NNW	Localized folds with west vergence; age relationship to D3 debatable
D1	S1 main continuous cleavage; mineral and shape fabric	L1 main linear fabric; mineral and extension lineation	F1 isoclinal folds with axial planar S1; complex geometry	NNW-trending fold axes, curved fold axes, and folded axial surfaces	Records main deformation in rocks with large finite strains observed locally; sheath folding in high-strain zone
D1a	Generally transposed into S1	Transposed into L1	Transposed isoclinal folds overprinted by D1 or seen as fold interference patterns	Complex; poorly resolved	Cryptic evidence of earlier fabric likely part of progressive deformation D1, producing sheath folds

Perspective views of 3D mapping on North Canyon Wall

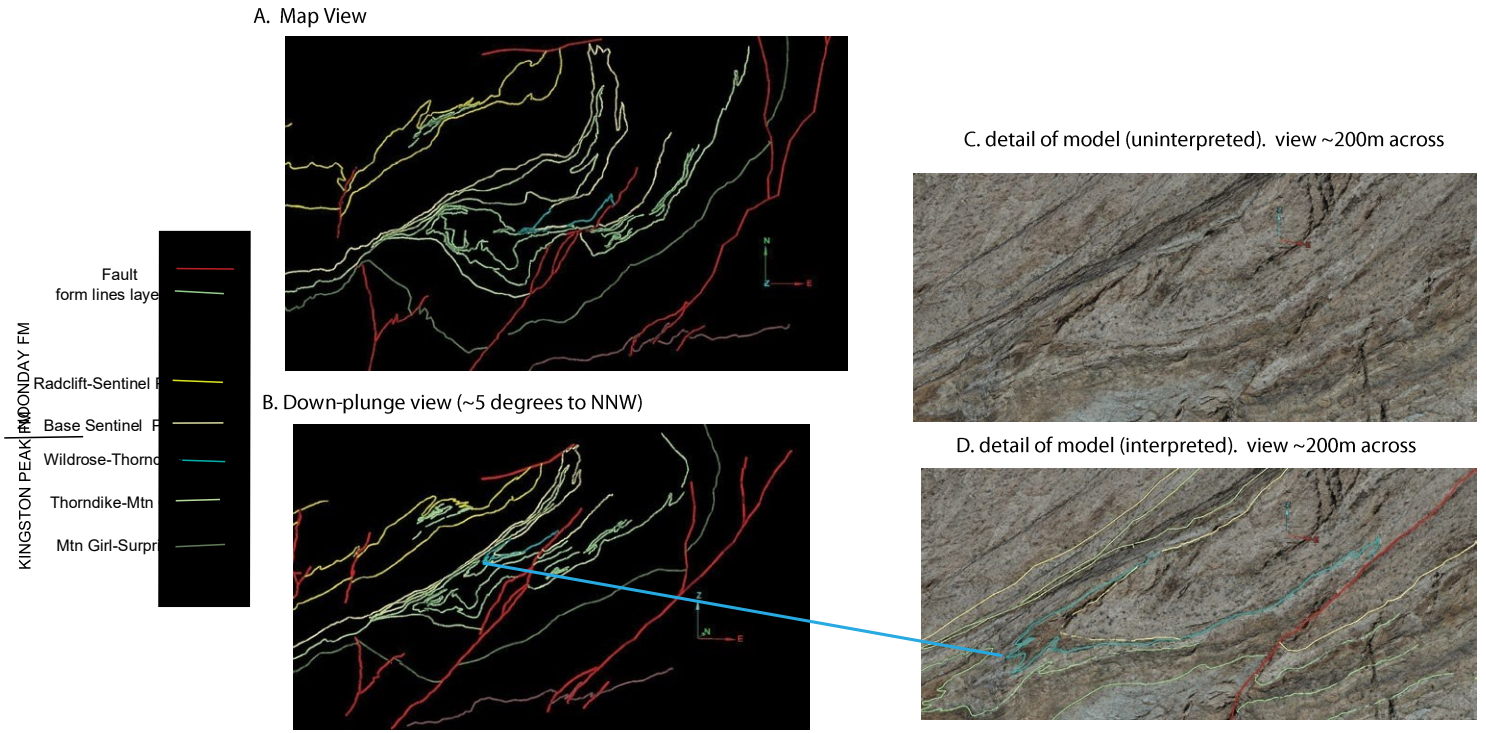

Figure 6. Screen captures of perspective views of three- dimensional (3-D) linework produced by direct mapping onto structure from motion– multiview stereo (SM) point cloud of north wall of Pleasant Canyon. (A) Map view. (B) Perspective view looking down plunge of the major isoclinal fold systems. (C, D) Uninterpreted and interpreted views, respectively, of main anticline- syncline pair along the Noonday Formation–K ingston Peak Formation contact illustrating high resolution of point cloud mapping base. Note terrain in this view is "benched" with vertical cliffs and sloped surfaces (benches). Blue line shows same point on the model and the interpretation for geographic reference. See 3-D PDF in Supplemental Material (see text footnote 1) to view these data in 3-D.

(S3) that is axial planar to mesoscopic folds that are similar in style to, and coaxial with, the macroscopic fold (Fig. 5).

On the eastern limb of the F3 synform, layering and layer-p arallel foliation are folded into a tight to close, nearly recumbent, gently inclined synform on the north canyon wall (section A-A′, Fig. 5; File S2). Across the canyon to the south (section B-B′, Fig. 5), this recumbent synform is the lower fold in a large antiform- synform pair that is asymmetric to the west (S- shaped looking north). The axial surface of this fold is nearly perpendicular to that of the F3 synform (Fig. 5). A number of smaller-s cale folds, particularly shown by the outcrop pattern of the Sourdough Limestone Member of the Kingston Peak Formation (Fig. 5), are interpreted as minor folds on this large-s cale fold system with S shapes looking north. Note that this asymmetry is consistent with a lower- limb position on the larger recumbent synform but inconsistent in structural style and asymmetry with the more open F3 synform. Based on projections of mapped contacts to the section lines (Fig. 5), the axial surface of the recumbent synform appears to be curved into an open fold geometry consistent with associated F3 folds in layering. This geometry is relatively well constrained from the 3-D mapping but could be deceptive because geometry is constrained by along- trend projection, which is subject to error in an area of 3-D structure like this one. We interpret this apparent curvature of the axial surface as refolding during F3, making the recumbent fold system F2 and west- vergent based on stratigraphic younging (Fig. 5). Nonetheless, this conclusion

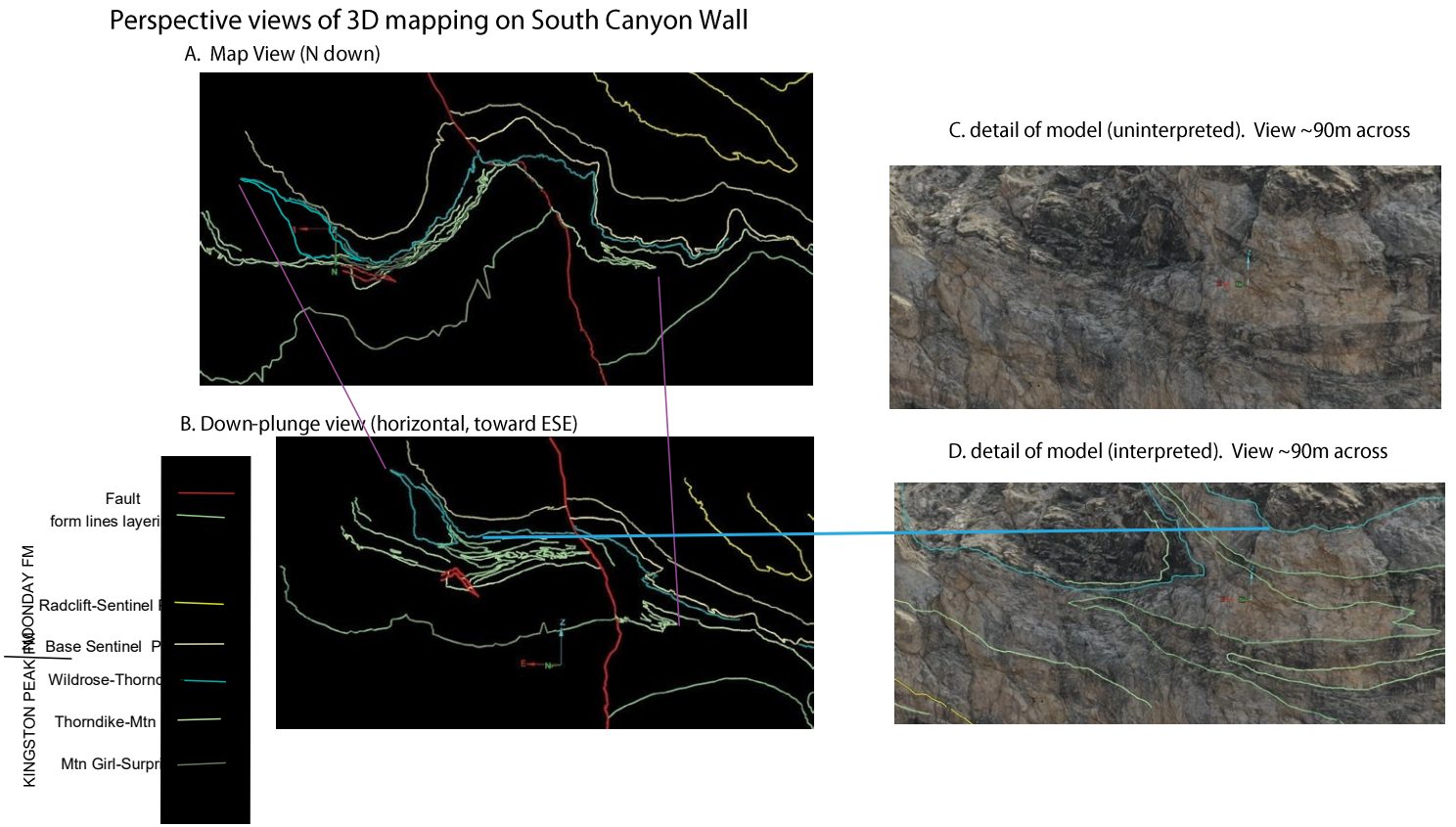

Figure 7. Screen captures of perspective views of three-d imensional (3-D) linework produced by direct mapping onto structure from motion–multiview stereo (SM) point cloud of south wall of Pleasant Canyon. (A) Map view. (B) Perspective view of model looking south along trend of fold axes. Note poor representation of structure in map view (A) due to vertical cliff of Thorndike Member marbles below Wildrose Member units (Kingston Peak Formation) versus clear visualization of structure in down- plunge view (B). Purple lines show equivalent points on the map view versus down- plunge view and blue lines show equivalent points between interpreted and uninterpreted model. (C, D) Uninterpreted and interpreted detailed views, respectively, of western closure of inferred sheath fold enclosing Wildrose diamictite. Note detail of point cloud at this scale. See 3-D PDF in Supplemental

Material (see text footnote 1) to visualize these features.

is tentative due to relationships in the lower part of the canyon that complicate this interpretation. This ambiguity is important because relationships in the lower part of the canyon complicate this interpretation.

This west- vergent F2 system overprints an even older, more complex fold system.

Most prominent is an isoclinal synform visible on a cliff face in marbles on the north canyon wall (section A-A′, Fig. 5; Fig. 6; Files S2 and S3). Brush et al. (2018) used a ground-b ased 3-D model of this structure to compare geometries on this cliff face deduced from a true 3-D model versus a 2.5-D model of the same structure. With new data from drone-b ased imaging used here, however, the details of this and related structures become clear. Specifically, our interpretation of this cliff face using the drone- based model (section A-A′, Fig. 5; Fig. 6; Files S2 and S3) is that the isoclinal synform described by Brush et al. (2018) is the lower syncline in an anticline- syncline pair. The syncline encloses the lower Noonday Formation (Sentinel Peak Member) in the Thorndike and/or Wildrose members of the Kingston Peak Formation, whereas the anticline encloses the Thorndike and/or Wildrose Kingston Peak units in highly deformed Sentinel Peak. Based on structural style and relative chronology, these isoclinal folds are clearly macroscopic manifestations of the F1- F1a succession observed at outcrop scale.

Finite strains are very high on the overturned limb of the fold pair, with dramatic thinning of stratigraphic units in this zone (Fig. 6; File S3). This observation suggests a distinct high-s train zone (shear zone?) along this horizon, which is supported by tracing the horizon westward from the fold pair where the zone cuts downward into the Mountain Girl (quartzite and conglomerate)
Member of the Kingston Peak, dramatically thinning the unit within the zone
(Figs. 4 and 5). These quartzites are accessible on the lower parts of the cliff, and high strains were confirmed by conglomerates with high- strain shape fabrics (Figs. 3A and 3B) and mylonitic textures seen in thin section. Indeed, strains are so high in the conglomerates that most deformed pebbles are stretched beyond resolution in maximum-s train sections (parallel to L and perpendicular to S), making quantitative strain estimates difficult. As an illustration, we were able to estimate strains in two principal sections of one sample (13tpp10): perpendicular to L and S (*Y/Z* section of strain ellipsoid) and perpendicular to S and parallel to L (*X/Z* section of the ellipsoid). Using harmonic mean of ellipticities (R) of ~40 objects per section, we estimate $R_{Y/Z}$ = 22 and $R_{X/Z}$ = 93. From these observations, we can calculate $R_{X/Y}$ (= $R_{X/Z}$ / $R_{Y/Z}$) = 4.2. This calculated ratio for *X/Y* would imply a strong flattening strain ($R_{X/Y} << R_{Y/Z}$), yet that observation is at odds with both the strong LS fabric in the rock (Fig. 4) and observations of a few stretched objects on the foliation plane with ellipticities >>4. Alternatively, we could assume based on the LS fabric that the strains are approximately plane strain. In plane strain, $R_{X/Y} = R_{Y/Z}$ and thus $R_{X/Z}^{calculated} = R_{Y/Z}^2$ or, for the values above, $R_{X/Z}^{calculated}$ = 501. This calculated value illustrates that the measured values on the *X/Z* section were almost certainly underestimated because strains that high are too large for routine measurement. Note that this estimated strain magnitude equates to a shear strain of ~23 in simple shear and is likely a minimum for the shear zone. That is, limestone marbles of the overlying Thorndike Member and dolomitic marbles of the Noonday Formation had undoubtedly much lower viscosity than these quartz-r ich metaconglomerates at this metamorphic grade (lower amphibolite facies), and thus, the strains are likely even higher in those structurally overlying marbles. This strain estimate is important because it is so high that normal 2-D structural assumptions are almost certainly invalid.

With the insight from the high strain magnitudes and the structural geometry of the isoclinal anticline-s yncline pair along the Kingston Peak–Noonday contact, we re-e valuated our initial interpretation of this structure (Brush et al., 2018), with our interpretation presented in cross- sectional representations of the structure in Figure 5 as well as visualizations of the model (Figs. 6 and 7; Files S2 and S3). The basis for the interpretation is as follows.

Immediately above the anticline-s yncline pair on the north canyon wall is a bold cliff

that is clearly composed of the Sentinel Peak Member of the Noonday Formation, but within these Sentinel Peak marbles is a dark carbonate band that pinches out to both the east and west into apparent fold closures (Fig. 5; File S2). We interpret this dark carbonate as the middle (Radcliff) member of the Noonday (Figs. 5 and 6). This interpretation is supported by indistinguishable dark carbonates that lie at the top of the cliff, in normal upright stratigraphic continuity with the Sentinel Peak marbles. Assuming this correlation is correct, the dark carbonates represent a synclinal closure within the Sentinel Peak cliff, but the hinges of that fold must be strongly curved to produce the double closure observed on the cliff (File S2). In this interpretation (Fig. 5), there is a second isoclinal fold closure above the anticline- syncline pair along the Kingston Peak– Noonday contact with a synclinal closure marked by the dark carbonates

(Sentinel Peak– Radcliff–S entinel Peak repeat) and a structurally overlying, cryptic anticline within the Sentinel Peak to return to the upright section at the top of the cliff. This interpretation is supported by observations on the ridgetop (Fig. 4), where lithologic outcrop patterns suggest fold interference patterns, but the details are difficult to resolve because of uncertainties in stratigraphic units within the Radcliff Member of the Noonday as well as poorly exposed contacts between quartzites and marbles that are nearly indistinguishable on imagery.

In the south wall of the canyon, similar fold structures are present but indicate further complexity along trend (section B-B′, Fig. 5; Fig. 7). On the lower slopes, Kingston Peak Formation units (Sourdough, Middle Park, and Mountain Girl) do not display significant internal structure aside from the D2-D3 deformation that folds foliation. Like in the north canyon wall, however, at the top of the Mountain Girl Member there is a dramatic thinning of the unit into a structurally higher, high-s train zone that marks a highly deformed band localized in the Thorndike limestone member and adjacent units (Fig. 7; File S2). Like in the north canyon wall, the Thorndike marbles display a series of isoclinal folds (Fig. 7) but lack the distinctive anticline- syncline pair enveloped in the Sentinel Peak Member (Noonday Formation). Instead, in the equivalent structural position of that fold pair, there is a syncline enclosing a dark band that we interpret as Wildrose diamictite enclosed in Thorndike marbles (both Kingston Peak Formation; blue lines, Fig. 7). These rocks are in turn structurally overlain by a cryptic anticline below a repeat of an upright section of Wildrose and Sentinel Peak (Figs. 5 and 7). We interpret this fold system as an equivalent anticline- syncline pair to the north wall structure (Fig. 6), but it is limited to older stratigraphic units (Thorndike and Wildrose). More importantly, however, the outcrop pattern of the Wildrose unit within the synclinal fold is lensoidal or eye shaped, similar to the syncline on the north wall that encloses Radcliff Member (Noonday) in Sentinel Peak, suggesting a similar geometry with strongly curved fold axes. Admittedly, this outcrop pattern could be a primary stratigraphic relationship along the unconformity, but the fold geometry is relatively clear on the western closure, strongly suggesting a fold origin. Finally, the fold complex along the Kingston Peak– Noonday contact is structurally overlain by a large- scale isoclinal syncline- anticline pair that encloses Radcliff within Sentinel Peak in the syncline and repeats Sentinel Peak across a cryptic anticline to an upright section at the top of the cliff (Files

S2 and S3), the same structural succession seen on the north canyon wall but lacking the lensoidal outcrop pattern of the syncline that encloses Radcliff.

Andrew (2022a) mapped a pair of detachment faults along approximately the position of what we show as the boundaries of a high-s train zone within the complex (Fig. 5). Andrew's (2022a) map has no accompanying text describing the detachment fault interpretation. Nonetheless, we reject this interpretation because there is no evidence of brittle deformation and the rocks are unequivocally a continuous metamorphosed stratigraphic succession, albeit thinned by finite strain, but lacking evidence of stratigraphic omissions. We presume the detachment interpretation arises from the thinning of units along this structural horizon. Nonetheless, the observed thinning does not require extension but can be produced by strain variations during flow, in either regional extension or contraction, with thinning of units produced by finite strain as the rocks were drawn into the flow in and out of the plane of the cliff faces.

Down- canyon (to west) from the marble- cored F3 synclinorium (Fig. 4), foliation rolls through a second large- scale F3 fold to form an anticlinorium comparable in wavelength to the synclinorium but with additional complexity

(Fig. 5). This fold was mapped by Andrew (2002, 2022a) and exposes lower Kingston Peak

Formation units (Surprise diamictite and interbedded volcanic units that are now amphibolite) as well as a deformed Cretaceous granitoid. Andrew (2002) dated this deformed pluton with conventional multi- zircon U-Pb methods and obtained a lower intercept age of 76.8 ± 0.8 Ma. He later reanalyzed the unit with chemical abrasion–t hermal ionization mass spectrometry (CA- TIMS) methods yielding an age of 82.536 ± 0.048 Ma (Andrew, 2022a). Andrew (2022a) interpreted the CA-TIMS date as a metamorphic age of a ca. 107 Ma granitoid based on correlation to a pluton dated by Cichanski (1995) using multi- zircon methods. Cichanski (1995) and Andrew (2022a) described a complex kinematic history for deformed Cretaceous leucogranites in the area, but in Pleasant Canyon, our observations indicate a single progressive deformation concentrated within and along the margins of the intrusion. Specifically, throughout lower Pleasant Canyon (cross section A-A′, Fig. 5), the granitoid is intensely deformed as evidenced by a mylonitic fabric with a moderately W- dipping foliation and a shallowly NW- plunging stretching lineation. Shear- sense indicators are ubiquitous in these rocks, with asymmetric porphyroclasts and S- C structure indicating a top-t o- the- NW shear sense (dextral-n ormal in modern coordinates) consistent with interpretations by Cichanski (1995). The contact between the mylonitic granitoid and underlying metasedimentary rocks is partially faulted (Fig. 4), but where the original contact is preserved the mylonitic fabric continues into adjacent schists as a distinct schistosity parallel to the mylonitic fabric. More importantly, however, within ~50 m of the contact, granitoid dikes of the same generation as the mylonitic granite are folded within the schists, and the schistosity is axial planar to folds developed in an older foliation. We interpret this older foliation as an S1 fabric, indicating that the overprinting fabric as well as the parallel mylonitic foliation in the granitoid are D2 or D3 fabrics or a different domainal fabric. Note that in amphibolites just to the east, this overprint is not conspicuous. Instead, the amphibolites show only a single, variably developed LS fabric defined by crystallographic amphibole alignments. In enveloping schists, however, the overprinting crenulation cleavage disappears within ~100 m of the granitoid contact. We suggest this observation indicates that the crenulation cleavage and mylonitic fabric in the granitoid represent a younger shear zone superimposed on the older fabrics, with a shear sense of top to the NW indicated by minor structures in the deformed granitoid. This shear zone apparently dies out within the schists of the Surprise Member and is virtually absent from underlying amphibolites due to relatively high viscosities of mafic rocks at these relatively low-g rade conditions. The age of this shear zone is no older than the Late Cretaceous age indicated by Andrew's (2022a) geochronology, but the minimum age is less well constrained. Moreover, even the relative age of this shear zone is unclear, a problem requiring additional study beyond that reported here.

The shear zone in the leucogranite and underlying schists is truncated to the west by a brittle, moderately west- dipping fault that juxtaposes metamorphosed Crystal Springs Formation and basement(?) against the metamorphic assemblage. Albee et al. (1981) referred to this fault as the South Park Canyon fault and interpreted it as a normal fault. Andrew (2022a) used Johnson's (1957) name of Goldbug fault for the structure to the south and interprets the hanging wall of this fault as highly metamorphosed Crystal Springs Formation, which is consistent with our interpretations and Cobb's (2015) geochronology. Andrew (2022a) used the juxtaposition of stratigraphic units along the Goldbug– South Park Canyon fault to infer a thrust fault that was reactivated as a normal fault in the Neogene. Although Andrew's (2022a) interpretation is allowable due to older-o n-younger juxtaposition of units, given the complexity of the metamor phic structures in the footwall and the kinematics of the deformation in the mylonitic granite, we interpret this fault as a dextral-n ormal system, consistent with conclusion of Cichanski (1995). Moreover, because the slickenlines on this fault are colinear with stretching lineations in the mylonitic granitoid, we infer that the fault and mylonitic deformation are part of a continuous deformation that progressed to brittle conditions. Note that the displacement on this fault and shear zone system plus displacements due to flow in structurally underlying rocks is significant because the presence of Crystal Springs Formation in the hanging wall is in marked contrast to the absence of Crystal Springs at the basement-c over contact at the eastern edge of our mapping (Fig. 4). In unmetamorphosed rocks to the east of Death Valley, the stratigraphic pinch- out of older Pahrump Group units across the basal Kingston Peak Formation unconformity occurs over several kilometers (Wright and Troxel, 1967). Thus, the stratigraphic discrepancy suggests significant displacements across the mapped area.

Remote Orientation Measurements from the Terrain Model

One of the potentially powerful applications of SM data is the ability to make remote orientation measurements on inaccessible parts of a field study site. The mining industry recognized this need long ago by developing remote measurement methods for dangerous active working faces where rock fall hazards were high. Commercial applications like Maptek PointStudio have widgets that can use point queries on a point cloud (lidar-b ased or SM-based) to estimate a best- fit plane to a suite of points, essentially the classic three- point problem of structural geology carried to *n* points where *n* can be a large number. This application has important potential in steep, inaccessible terrain, but our initial experience with these methods implies a need to use these methods with caution (e.g., Brush et al., 2018; T. Pavlis, unpublished observations from student researchers, 2013–2020). Thus, in conjunction with our analysis of the structure in Pleasant Canyon, we performed an experiment on remote orientation analysis, focused on the F1 recumbent syncline- anticline pair on the north wall of the canyon (Fig. 6; File S2). Orientation analysis on an isoclinal fold of this type is a challenge, even in a traditional field study, but our result here suggests great caution is needed in use of digital data like those used here.

Figure 8 illustrates the results of this experiment in the context of orientations measured in the field. The field data are from the entire study area of Figure 4 and show the basic geometric relationships described above (in the Mesoscopic Structure section) where the primary foliation is folded about subhorizontal, approximately N- S axes (both F2 and F3), scattering poles to foliation along a great circle consistent with folding. The fold axes are also subparallel to the extension lineation (red dots in Fig. 8A)

The lower part of Figure 8 illustrates the result of the remote measurement experiments. Figure 8C shows all the remote measurements obtained from a single

session using the tools in PointStudio. The only quality control exercised in these remote measurements was culling of measurements that were clearly >20°–30° from a qualitative assessment of layering orientation. Note that in PointStudio this is straightforward because the program shows a disc in the visualization, which can be manipulated with the scene to evaluate the accuracy of the measured orientation. As expected, poor measurements that were immediately rejected this way were sites where the picked points were relatively linear, leading to large errors when a plane was fit to these data. Even with this culling method, however, the resultant data set (Fig. 8C) is surprisingly scattered. Specifically, in this fold pair, the hinge line of the syncline is exposed on the cliff face, allowing direct measurement of the fold axis on the model (large blue dot on Figs. 8C– 8E), yet the scatter of the poles to layering measured remotely would suggest a fold axis nearly 90° from the observed axis (shallow plunge to the SW rather than the observed shallow NW trend; Fig. 8C). To evaluate this issue, we re- evaluated the orientation data as a stand- alone visualization, without the distraction of the point cloud scene from which it was derived. In that perspective, by manipulating the scene, it became apparent that clusters A and B in Figure 8C were errant measurements that deviated significantly from adjacent measured orientations. Thus, we then re- evaluated the data and picked what appeared to be characteristic measurements for each limb of the syncline, a pair which should, in theory, yield a fold axis orientation at the intersection of the two great circles on a stereonet plot. That analysis (Fig. 8D) also yielded an incorrect result, nearly 90° from the known fold axis. Finally, with the failure in two- point analysis, we plotted multiple “select data” that appeared to represent the two limbs of the fold well, and the result (Fig. 8E) is more satisfying, i.e., a spread of great- circle intersections that broadly fit the observed fold axis trend.

This analysis is shown in detail here because it illustrates that remote orientation

analysis can be a powerful tool but must be applied with care and must be combined with quality control analysis at various levels. In traditional studies with field measurements, the field geologist does this type of quality control “on the fly” in the field. For example, an errant measurement can generally be recognized quickly by comparison to nearby measurements, and measurement errors can be minimized by contouring the data (e.g., Fig. 8a), particularly where the number of measurements is large. The example shown here is a virtual measurement equivalent of this procedure. We eliminated obvious outliers “on the fly” by discarding the measurements, but more subtle measurement errors were not eliminated by this method. Instead we had to examine the data more closely in a 3-D visualization, which revealed the fundamental problems and the likely solution (Figs. 8D and 8E). That is, because the fold is isoclinal, even small errors in the measured orientations can product significant errors in the analysis, even when the best data are sorted for analysis. Thus, although a single-p air analysis failed (Fig. 8D), pooling of multiple high- quality measurements provided a better assessment (Fig. 8E). Note that this type of visualization analysis of the orientation data would be impossible in conventional paper-b ased geologic mapping, and even in 2-D digital environments requires an extra step, e.g., 2.5- D analysis in a Google Earth–b ased widget (Whitmeyer and Dordevic, 2023) or use of high- end software like MOVE from Petroleum Experts.

DISCUSSION

Synthesis of Field Observations

Structures in the Panamint metamorphic complex other than folds in foliation (F2 and F3) have been overlooked or disappear at map scales smaller than 1:24,000 (e.g., Albee et al., 1981; Labotka et al. 1980; Andrew, 2022a), giving a false impression that the structure of the complex is a simple homocline or weakly folded assemblage. Structural analysis at larger scales that includes full 3-D analysis from high- resolution terrain models reveals macroscopic fold systems at scales of 100– 400 m with structural geometries consistent with mesoscopic fabrics indicating four to five phases of ductile deformation. The earliest folds (F1a and F1) show fold interference patterns that represent a fold overprint, sheath folding, or both. Given the large strain magnitudes recognized in one sample from the high- strain zone, sheath folding is not only allowable but highly likely. D1a and D1 formed the main continuous cleavage, which is in turn overprinted by two generations of folding: F2 produced domainal, recumbent folds and F3 produced upright, horizontal to gently inclined folds. A dextral- normal ductile shear zone developed atop the metamorphic assemblage, fully involving a Late Cretaceous granitoid with a mylonitic fabric extending structurally downward as a crenulation cleavage developed on the older schistosity (S1-S 1a composite), but no direct overprints were observed to establish whether this crenulation cleavage represents S2 or S3. The dextral- normal shear zone has kinematics consistent with slickenlines developed along a brittle fault that caps the shear zone, suggesting

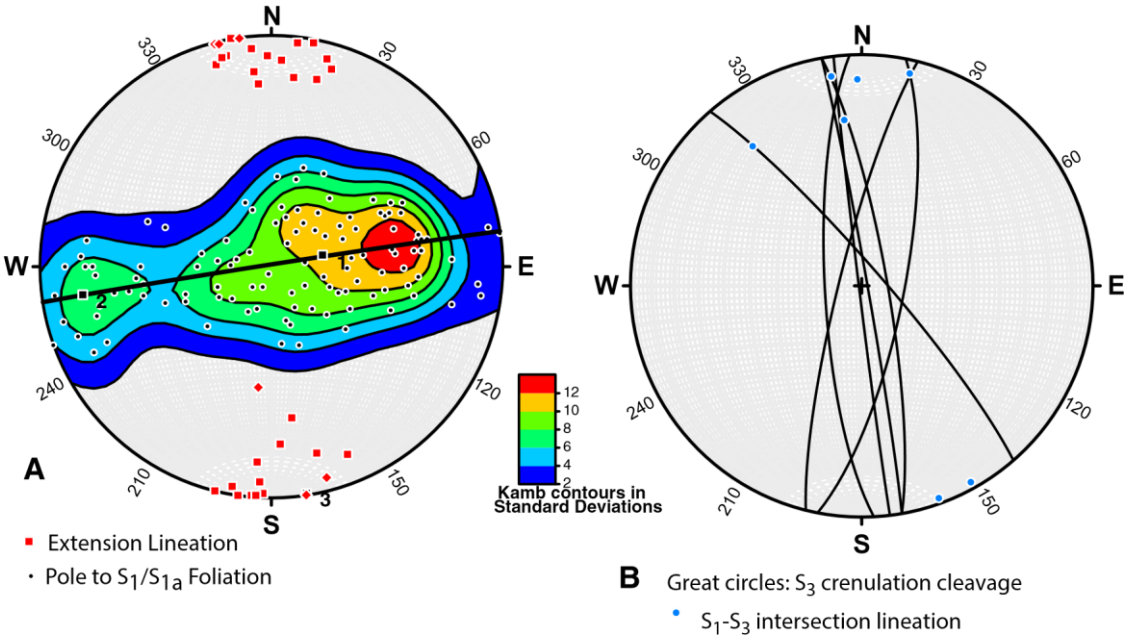

FIELD MEASUREMENTS:

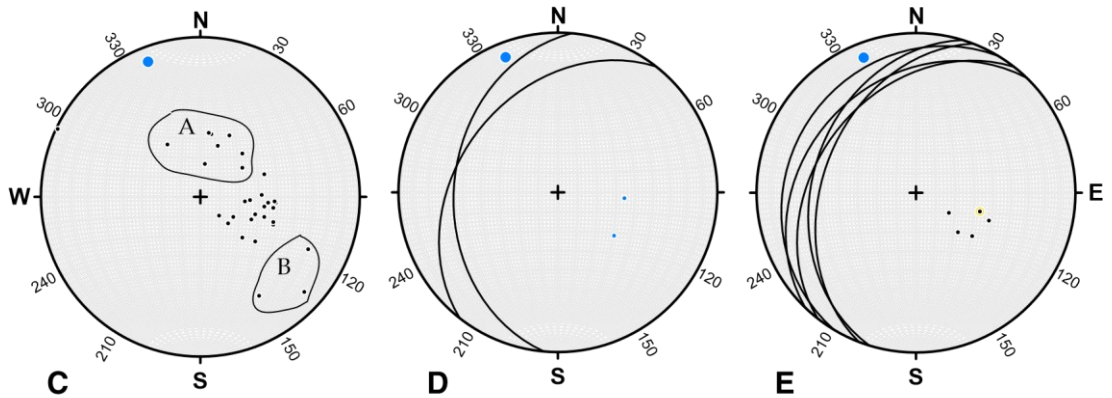

ENTIRE FIELD AREA REMOTE MEASUREMENTS:

ISOCLINAL SYNCLINE IN THORNDIKE MARBLES

Figure 8. Equal- area stereographic projection plots of orientation data from field site comparing field

measurements (top) and orientations obtained from model by remote, multipoint analysis on the isoclinal fold in Thorndike Member marbles (Kingston Peak Formation) visualized on north canyon wall (below). (A) Main- phase fabric elements (S1 foliation, black dots and contours; extension lineations, red dots). (B) Crenulation cleavage (great circles) and S1- S3 intersection lineation (blue dots). Note cylindrical fit of foliation poles (great-c ircle distribution) matches both extension lineation and F3 fold axes (S1-S 3 intersection) showing that the great- circle distribution of foliation poles reflects observed F3 folds. (C– E) Results of remote orientation measurements of layering, illustrating potential pitfalls in the method. Large blue dot is fold axis measurement made directly on the model. C shows all remote measurements shown as poles to planes with groupings A and B representing clusters not anticipated from geometry that would produce an incorrect geometric analysis (see text); B shows initial guess of two "best planes" by selecting a single orientation pair from two limbs of the syncline; D shows group of measurements judged "best" by visual inspection on the three-dimensional visualization of orientation data. See text for discussion.

the shear zone and fault are part of the same dextral- normal system. Thus, although this fault places older rocks over younger, it is a dextral- normal fault, not a thrust fault, and is tentatively assigned to a fourth generation (D4) of deformation (Table 1).

Sheath Fold Interpretation

Our field observations and 3-D mapping provide new perspectives on the Mesozoic, syn-m etamorphic history of the Panamint Range. The picture of the internal structure of the Panamint Range portrayed by Labotka et al. (1980) and Albee et al. (1981) is an oversimplified view and has contributed to misconceptions that have carried through to tectonic syntheses that are clearly incorrect (e.g., Norton, 2011). Our conclusions are broadly consistent with work both to the north (Hodges et al., 1987) and in the central to southern Panamint Range at regional scale (Andrew, 2002, 2022a, 2022b) but with important distinctions revealed by detailed 3-D mapping.

The earliest phases of the ductile deformation generated both D1a and D1 fabrics. At mesoscopic scale, F1 isoclinal folds are common and conspicuous, but F1a structures are commonly rootless folds that are variably transposed into the continuous cleavage, S1-S1a. Both F1 and F1a axes, however, generally are subparallel to a prominent NNW-trending stretching lineation. Thus, either these folds formed with axes parallel to stretching or the axes were rotated into parallelism with flow lines, i.e., F1 and F1a are manifestations of a single progressive deformation and are sheath folds. Local exposures show type 1 and type 3 fold interference patterns that could have been produced by overprinting, sheath folding, or both.

We suggest that the Pleasant Canyon cliff faces are a macroscopic “Rosetta stone”

linking the mesoscopic observations to macroscopic scale and support an interpretation that the D1-D 1a succession is primarily the product of a single progressive deformation dominated by sheath folding. Specifically, the outcrop patterns of folded layering in Pleasant Canyon suggest strongly that the fold systems are noncylindrical with curvilinear hinges at macroscopic scale. The most significant observation supporting the conclusion is the lensoidal outcrop pattern of Radcliff Member enclosed in Sentinel Peak Member (Noonday Formation) on the north canyon wall and Wildrose Member enclosed in Thorndike Member (Kingston Peak Formation) on the south wall, both suggesting an eye-fold geometry with axes that curve to form a dome- and- basin geometry. This geometry can originate from superposition of two generations of folds with nearly perpendicular axes (type 1 interference pattern of Ramsay, 1967). Indeed, given the location of the Panamint metamorphic complex in a sharp bend in orogenic trend with a complex history (Fig. 1), overprinting to produce these fold systems certainly would have been possible. Nonetheless, the close parallelism between fold axes and the stretching lineation as well as the apparent sense of fold axis curvature both suggest that this geometry is the product of large- scale sheath folding during a single progressive deformation. Sheath folding has long been recognized as a product of progressive strain, particularly in shear zones where finite strains accumulate rapidly (e.g., Ramsay and Graham, 1970). Specifically, whenever strain ellipsoids show maximum ellipticities >10, sheath folding becomes increasingly likely (e.g., Ramsay, 1980; Fossen and Cavalcante, 2017). Based on strain estimates from the site in the Mountain Girl Member (Fig. 5), that criterion is easily met in the inferred shear zone in Pleasant Canyon where maximum axial ratios are clearly >100 and possibly as high as 500 in Kingston Peak metadiamictites and metaconglomerates. Given this evidence for very high strains in quartz-r ich rocks and the general observation that marbles are weaker than metapsammites at amphibolite facies conditions (e.g., Brodie and Rutter, 2000), the finite strains in the Pleasant Canyon marbles are likely even higher than the metapsammites. Moreover, experimental and field observations also suggest that dolomite marbles, like those in the Sentinel Peak Member, are as weak or weaker than limestone marbles at this grade (Delle Piane et al., 2008), consistent with the observed evidence of high strain continuing into dolomite marbles in Pleasant Canyon. Thus, sheath folds are not only allowable but are likely. We interpret the F1- F1a folds in Pleasant Canyon as sheath folds generated during a single, progressive deformation in the Mesozoic.

The interpretation of these folds as sheath folds and their localization along the Kingston Peak–N oonday contact also suggests strongly that there is a high- strain zone localized along that contact. That inference would not be surprising given calcite and dolomite marbles are well known to be relatively low- viscosity rocks at these grades (Brodie and Rutter, 2000; Delle Piane et al., 2008) and the Thorndike Member of the Kingston Peak Formation and the Noonday Formation are dominantly calcite and dolomite marbles, respectively, between quartz- rich clastic units. Thus, we suggest that a major D1a- D1 shear zone localized in the calcite marbles along the Kingston Peak–N oonday contact, but dispersed strain along the zone spread into the underlying quartzite and conglomerate Mountain Girl Member (Kingston Peak) as well as the overlying Noonday dolomite marbles and quartzites. Shear- sense indicators are not obvious in these rocks, but that observation is not surprising because determining shear sense in polyphase tectonites, particularly marbles, is always difficult. Note that microstructure studies of the quartz-r ich rocks would likely resolve this issue and should be considered in future work.

Significance of Sheath Folding within the Metamorphic Complex

The measured strains at one site in Pleasant Canyon indicate very high strains, and if our inference of even higher strains in marbles is correct, the displacement across the shear zone is significant. Specifically, the structural thickness of the apparent shear zone (Fig. 5) is ~200–2 50 m. Using the measured strain value and an assumption of plane strain, a shear strain of 23 would indicate a minimum displacement of 4600– 5750 m across the zone. However, if the strains in the marbles are much higher, the displacement across the zone could be in the tens of kilometers, and even larger offsets are possible.

Clearly these large offset estimates are speculative but illustrate the potential significance of the structure. Even an offset of 4–5 km is a significant offset within a system that is often assumed to be a simple homocline, but offsets in the tens of kilometers imply an even greater significance for the internal structure of the metamorphic complex. In particular, this structure is cryptic at map scale and is invisible to conventional lithologic mapping where juxtaposition of rock units or repetition by macroscopic folds is the main criterion used for recognizing major structures.

More work is needed to clarify the potential displacement magnitudes, but our observations here beg a number of questions. First, the evidence that displacement occurred largely along primary sedimentary layering suggests this high- strain zone may be a décollement level for the Mesozoic thrust systems of the Sevier belt. If true, this exposure may be an unusual exposure of a major feature known from virtually all thrust belts but rarely seen at Earth's surface. If the latter is also true, how many other high-strain zones have been overlooked within a metamorphic complex that appears to a simple homoclinal stratigraphic succession? Finally, Neogene extensional magnitudes have been constrained largely by reconstructing Mesozoic thrust systems in this region. How does a high- strain horizon(s) within the complex affect these interpretations if there is a horizon(s) that have accommodated tens of kilometers of thrust offsets transferred to the foreland but are nearly invisible in the hinterland metamorphic complex?

The D2-D3 Problem: What Do the Overprints Represent?

More work is needed to clarify both the relative and absolute age of crenulation cleavages in the Panamint metamorphic complex. From mesoscopic fabric observations throughout the metamorphic complex, the most prominent and widespread overprint on the primary fabric is a steeply dipping crenulation cleavage with associated upright folds (Fig. 3G). This cleavage is clearly coeval with ubiquitous, upright folds developed throughout the Panamint Range that have been known for decades (e.g., Labotka et al., 1980; Albee et al., 1981). Although we place these fold systems in a third deformational event (D3), that chronology is not directly constrained by overprints seen at outcrop to hand- specimen scale. The only constraint on the relative age of the upright folds (F3) and recumbent folds (F2) is apparent curvature of axial surfaces of the recumbent folds into

upright forms consistent with F3 refolding. Although allowable, that relative age is an interpretation, and it is possible the axial surface curvature results from other geometric complications.

This issue becomes clearer through consideration of our observations from the shear

zone along the Goldbug– South Park Canyon fault. There, a mylonitic shear zone is clearly developed in the footwall of the fault with a shear sense compatible with slickenlines on the brittle fault, an observation suggesting strongly that the fault and shear zone record phases of the same continuous deformation that progressed from ductile to brittle. This type of fabric- fault association is characteristic of extensional shear zones in metamorphic core complexes (e.g., Davis and Coney, 1979; Wernicke and Burchfiel, 1982; Tirel et al., 2008; Platte et al., 2015). Thus, we conclude this shear zone and capping fault record a post–ca. 70 Ma transtensional event, but how this event fits into the observed ductile overprints remains debatable. Specifically, the observation that the mylonitic fabric of the Cretaceous granitoid extends structurally downward into a crenulation cleavage in schists begs the question: Which, if either, of the observed fabric overprints is associated with this shear zone?

Given the regional history, the simplest interpretation would be to equate the youngest fabrics (D3 structures) with the shear zone, yet D3 is kinematically incompatible with the known kinematics of the shear zone. That is, in modern coordinates, D3 records approximately E- W compression and subvertical extension, whereas the shear zone records subhorizontal, NW extension and a steeply plunging shortening axis. D2 structures, in contrast, are kinematically compatible with the shear zone—steeply dipping shortening axis with unresolved extensional direction but likely perpendicular to approximately N- S fold axes. Nonetheless, if our inferred relative chronology is correct, the structural geometry of F2 and F3 folds in Pleasant Canyon is incompatible with the recumbent folds being formed during motion on the shear zone.

Based on this reasoning, we suggest that the most likely scenario is that the observed overprint seen in schists structurally below the mylonitic granitoid records yet another structural overprint, spatially limited to a narrow shear zone beneath the Goldbug–S outh Park Canyon fault. We tentatively refer to this event as D4 (Table 1) and conclude it records the development of a distinct, core complex–t ype transtensional shear zone that deformed only a narrow zone along the shear zone. The age of the structure is debatable but likely is Late Cretaceous given that: (1) it is no older than the granitoid that is fully involved in the deformation (dated by Andrew [2022a] at 82.536 ± 0.048 Ma); (2) it is almost certainly older than Ar- Ar mica cooling ages from nearby schists that scatter between 66 and 80 Ma (Labotka et al., 1985); and
(3) it is unequivocally older than Zr (U-Th)/He dates in the central Panamint Range that range from ca. 10 to 50 Ma (Bidgoli et al., 2015), although that age range demonstrates little other than Neogene exhumation along the present western boundary normal fault of the range.

We suggest that resolving the kinematics and absolute timing of the overprints in the western Panamint Range is an important problem for regional tectonics. The Goldbug–South Park Canyon shear zone and fault is probably part of the same structure that follows the mountain front from Wildrose Canyon to well south of the study area, the structure that Albee et al. (1981) mapped as the Surprise fault. A Late Cretaceous age for this structure is likely and may be part of a regionally recognized history of Late Cretaceous extension first well documented in the Funeral Mountains east of Death Valley (e.g., Applegate and Hodges, 1995). Assuming D2 and D3 are manifestations of even older deformation, they also record important regional events, but how they tie to nearby structures is subject to refinement of their absolute age. D3 structures clearly fully involve Late Cretaceous granitoids elsewhere in the complex (e.g., Cobb, 2015; Subia, 2019), but how they link to the Goldbug–S outh Park Canyon fault system remains unclear. D3 is clearly too young to associated with the Late Jurassic Eastern Sierran thrust system to the west described by Dunne and Walker (2004). Instead, D3 records Laramide- age deformation as seen to the east (Pavlis et al., 2014) although D3 in the Panamint Range is kinematically distinct with E- W- rather than N- E- directed shortening. D2 is even more cryptic, with no clear links to regional geology and little information on even local relative chronology.

3-D Mapping: An Important New Method for Resolving Complex Structure

We suggest that without the aid of 3-D visualizations afforded by our detailed SM models, the inference of macroscopic structure in Pleasant Canyon would have been difficult to impossible. There are several reasons for this suggestion.

First, conventional 2-D mapping would have, at the least, failed to recognize geometric details and, at the worst, would never have recognized the structural complexity. This conclusion is demonstrated by existing published
2-D maps: fixed scale, paper-b ased maps produced by Albee et al. (1981) and Cichanski (1995) and a 2-D map produced using orthoimagery in GIS-b ased digital mapping by Andrew (2022a). This observation is not a criticism of these maps given that all geologic mapping evolves with increasing information obtained over time, but we submit that both of these mapping efforts were handicapped by basic limitations of a 2-D map base that limited their ability to resolve structure. Specifically, the steep terrain of the Pleasant Canyon area is a major handicap to resolving structure with a 2-D map base because the cliff faces, where most of our critical observations are made in this study, are virtually invisible on a 2-D map (e.g., Figs. 6 and 7). Thus, even the most accurate 2-D mapping of cliff faces would obscure details like those used to resolve structures in Pleasant Canyon.

Second, mapping scale was likely a handicap to previous mapping in this terrain. The paper maps of Albee et al. (1981) and Cichanski (1995) were fixed- scale maps, generated by mapping onto photo enlargements of 1:24,000- or 1:62,500-s cale topographic maps, and structures described here are too small to be represented at that scale. Even the digital mapping of Andrew (2022a) likely suffered from scale issues because although digital mapping allows a wide range of zoom levels, imagery resolution together with the steep terrain undoubtedly affected the ability to resolve these relatively small features. This implies that elsewhere, key features like those described here have been missed during conventional geologic mapping.

Third, and perhaps most important, is that 3-D visualizations afford a luxury for

structural analysis that is impossible in conventional studies by allowing unlimited time to analyze features from an unlimited range of look angles. It is hard to overemphasize how important this ability can be in an analysis of structures as complex as the features we describe here. Based on our many years of experience in field studies, that ability to repeatedly view a scene from many angles cannot be replicated in a field environment, where all analyses are rushed in comparison and a range of look directions would be impossible to achieve without use of aviation (e.g., a helicopter).

Remote Orientation Measurement: A Valuable Tool but Caution Is Needed

A frustration of many field studies is an inability to obtain orientation data on inaccessible cliffs. SM models resolve this problem with important caveats. Multipoint picking tools can allow remote measurements of layering via an extension of the familiar three-p oint problem, but our analysis here suggests even a skilled interpreter can produce data that are at best misleading and at worst could lead to an incorrect assessment (Fig. 8). Our problems arose in large part because the exposures used for orientation analysis suffered from large areas of 2-D exposure—nearly planar cliff faces. This problem is not uncommon. In addition, the scale of the structures relative to the model as well as the isoclinal fold geometries exemplified measurement errors. Some of these problems could have been addressed partially by obtaining more measurements and using conventional techniques like contouring data. Nonetheless, obtaining more data in this case may have been counterproductive because we emphasized measurements at sites where exposures appeared sufficiently 3-D to allow an accurate measurement. It is likely that a relatively unskilled observer would have produced an even more unsatisfactory result in this analysis.

We suggest that the solution to this problem is probably different under different conditions. In an area with ledgy outcrops where the ledges represent layering surfaces, this type of analysis is likely highly accurate. Indeed, Brush et al. (2018) presented an example, from this same area, that showed the technique was much more successful on ledgy exposures than on the cliff face we analyzed here. In areas like the one analyzed here, it appears remote measurements should be viewed with caution and carefully analyzed with 3-D visualizations to obtain satisfactory results in orientation analysis. Based on the success of sorting data into suites of highest- quality measurement using the 3-D visualization, that method should be further analyzed. Nonetheless, we suggest that all remote measurements of this type need to be carefully compared both within the data set itself and using field measurements to confirm their accuracy.

Recommendations for Future Studies

Techniques used here can be easily extended to a variety of field studies and, in our opinion, should become the norm for mapping geologic structure in areas of significant topographic relief. Here we illustrate an application of the method at an intermediate scale between most conventional map scales and virtual outcrop scales. Based on the experience here, this scale may be critical in the resolution of a range of geologic problems. That is, in areas where the structures have scales of a few hundred meters, significant features may be overlooked as “too small to map” with conventional methods, but when such features are overlooked, an important element of the structure is missed. With the widespread availability of drones, studies like ours should become routine for analysis of features in this scale range.

More importantly, however, the methods used here can be easily extended to larger regions through a different acquisition method: imaging using a crewed aircraft. In this method, it is possible to acquire standard vertical aerial photography, but in steep terrain, a superior method is to acquire images as the aircraft flies along an escarpment or down a steep-w alled valley, with handheld cameras acquiring images on one or both sides of the aircraft, depending on the situation. Rutkofske et al. (2022) showed an example of using this method to resolve complex structure where the rock units were highly faulted but showed layering at submeter to meter scales, which was easily resolved at the model resolution of 20–3 0 cm (Pavlis and Serpa, 2023). One of us (Pavlis) has spent years working in steep- walled, glaciated valleys in Alaska, and had this technology been available during that work, our structural studies would have been both easier to accomplish and likely far more complete. This is particularly true in remote sites like in Alaskan studies, where aviation is routinely used for access to field sites. Thus, adding a photogrammetry flight to an aircraft charter would be a trivial expense in comparison to the value added in employing SM and 3D mapping techniques. We believe *all* future studies in remote sites with steep terrain that require access by aviation should automatically devote some time to SM data acquisition and make use of this technology. Moreover, we suggest that large organizations like geological surveys should formalize SM data acquisition in areas of steep terrain, including development of acquisition systems that automate data acquisition with vertical and oblique imagery acquired simultaneously. Such a system could be easily combined with lidar data acquisition to produce spectacular visualizations and new resolution of geologic problems.

CONCLUSIONS

SM technology has the potential to revolutionize field studies by providing a high-r

esolution, 3-D colored model that can serve as a base for true 3-D mapping on surfaces that are vertical or even overhanging. This can allow unprecedented mapping detail with resolutions to the centimeter level over scales of kilometers. We show an example where a drone-b ased model of cliff- face exposures revealed structures that would have been at the least distorted (Figs. 6 and 7) and likely invisible on conventional 2-D maps. Interpretation of these models suggests that in the study area, isoclinal fold systems are noncylindrical, with dome- and- basin fold geometries where dome and basin axes are parallel to extension, a geometry highly suggestive of sheath folds at large scale and supported by observed large finite strains. The scale of these structures, however, even on a 2-D map, would likely be overlooked at typical scales of conventional mapping (~1:20,000– 1:50,000), indicating drone- based models represent a frontier for new discoveries in structural geology. Remote orientation measurements are also possible using these models but should be used with caution because significant measurement errors arise from exposures with insufficient 3-D geometry. We suggest a quality-c ontrol approach using both culling in real time while measurements are acquired and data sorting into high- versus low-q uality measurements using 3-D visualization of the planar measurements without distraction of the underlying point cloud.

3-D mapping methods should be extended to larger areas using conventional aircraft. Large areas of the Earth, particularly at high latitudes, are difficult or impossible to access on foot. These areas are superb candidates for using SM technology to develop 3-D map bases on cliff walls, particularly in glaciated valleys, and these data could be acquired with minimal, if any, additional cost to a field effort that already is using aviation for access.

More work is needed, particularly focused geochronologic studies, to determine the absolute age and kinematics of structural overprints in the Panamint Range metamorphic complex. The Goldbug–S outh Park Canyon fault and associated shear zone represents a transtensional or extensional shear zone of likely Late Cretaceous age, but two overprinting fabrics observed within the metamorphic complex are probably distinct events that require clarification on age and kinematics.

ACKNOWLEDGEMENTS

This work was supported by U.S. National Science Foundation grant EAR 2049603 to the authors. We express special thanks to Mauro Alberti who within days added features to the qProf plugin in QGIS when we discovered the plugin initially did not take advantage of true 3-D linework but relied on line drapes onto a digital elevation model (DEM). Work by students Josh Cobb, Jade Brush, Tai Subia, Zach Fleming, James Rutkofske, and Valeria Martinez laid the foundation for this study, and we thank them for their efforts, including field collaborations. We also thank colleagues Richard Langford and Jose Hurtado for years of collaboration on developing digital mapping techniques. We thank Joe Andrew and an anonymous reviewer for insightful reviews that helped focus the manuscript.

REFERENCES CITED

Albee, A.L., Labotka, T.C., Lanphere, M.A., and McDowell, S.D., 1981, Geologic map of the Telescope Peak quadrangle, California: U.S. Geological Survey Geologic Quadrangle Map GQ- 1532, scale 1:62,500, https:// doi .org /10 .3133 /gq1532.

Andrew, J.E., 2002, The Mesozoic and Tertiary tectonics of the Panamint Range and Quail Mountains, California [Ph.D. thesis]: Lawrence, University of Kansas, 387 p.

Andrew, J.E., 2022a, Geologic map of central Panamint Range, California, USA: Geosphere, v. 18, p. 730– 731, https:// doi .org /10 .1130 /GES02344 .1.

Andrew, J.E., 2022b, Geologic map of southern Panamint Valley, southern Panamint Range, and central Slate Range, California, USA: Geosphere, v. 18, p. 726– 727, https:// doi .org /10 .1130 /GES02342 .1.

Andrews, G.D.M., Labishak, G.D., Brown, S.R., Isom, S.L., Pettus, H.D., and Byers, T., 2020, Teaching with digital 3D models of minerals and rocks: GSA Today, v. 30, no. 9, p. 42–4 3, https:// doi .org /10 .1130 /GSATG464GW .1.

Applegate, J.D.R., and Hodges, K.V., 1995, Mesozoic and Cenozoic extension recorded by metamorphic rocks in the Funeral Mountains, California: Geological Society of America Bulletin, v. 107, p. 1063– 1076, https:// doi .org /10 .1130 /0016 -7606 (1995)107 <1063: MACERB>2 .3 .CO;2.

Bemis, S.P., Micklethwaite, S., Turner, D., James, M.R., Akciz, S., Thiele, S.T., and Ali Bangash, H., 2014, Ground- based and UAV- based photogrammetry: A multi-s cale, high- resolution mapping tool for structural geology and paleoseismology: Journal of Structural Geology, v. 69, p. 163– 178, https:// doi .org /10 .1016 /j .jsg .2014 .10 .007.

Bidgoli, T.S., Amir, E., Walker, J.D., Stockli, D.F., Andrew, J.E., and Caskey, S.J., 2015, Low- temperature thermochronology of the Black and Panamint mountains, Death Valley, California: Implications for geodynamic controls on Cenozoic intraplate strain: Lithosphere, v. 7, p. 473– 480, https:// doi .org /10 .1130 /L406 .1.

Brodie, K.H., and Rutter, E.H., 2000, Deformation mechanisms and rheology: Why marble is weaker than quartzite: Journal of the Geological Society, v. 157, p. 1093–1 096, https:// doi .org /10 .1144 /jgs .157 .6 .1093.

Brunier, G., Fleury, J., Anthony, E.J., Gardel, A., and Dussouillez, P., 2016, Close- range airborne Structure- from-Motion Photogrammetry for high- resolution beach morphometric surveys: Examples from an embayed rotating beach: Geomorphology, v. 261, p. 76– 88, https:// doi .org /10 .1016 /j .geomorph .2016 .02 .025.

Brush, J.A., 2015, Evaluating methods of field- based 3D visualizations and their applications to mapping metamorphic terranes: an example from the Panamint Mountains, California [M.S. thesis]: El Paso, University of Texas at El Paso, 124 p.

Brush, J.A., Pavlis, T.L., Hurtado, J.M., Mason, K.A., Knott, J.R., and Williams, K.E., 2018, Evaluation of field methods for 3-D mapping and 3-D visualization of complex metamorphic structure using multiview stereo terrain models from ground- based photography: Geosphere, v. 15, p. 188– 221, https:// doi .org /10 .1130 /GES01691 .1.

Burchfiel, B.C., and Davis, G.A., 1972, Structural framework and evolution of the southern part of the Cordilleran orogen, western United States: American Journal of Science, v. 272, p. 97–1 18, https:// doi .org /10 .2475 /ajs .272 .2 .97.

Burchfiel, B.C., Hamill, G.S., IV, and Wilhelms, D.E., 1983, Structural geology of the Montgomery Mountains and the northern half of the Nopah and Resting Spring Ranges, Nevada and California: Geological Society of America Bulletin, v. 94, p. 1359–1 376, https:// doi .org /10 .1130 /0016 -7606 (1983)94 <1359: SGOTMM>2 .0 .CO;2.

Burchfiel, B.C., Hodges, K.V., and Royden, L.H., 1987, Geology of the Panamint Valley–S aline Valley pull- apart system, California: Palinspastic evidence for low-a ngle geometry of a Neogene range- bounding fault: Journal of Geophysical Research: Solid Earth, v. 92, p. 10,422– 10,426, https:// doi .org /10 .1029 /JB092iB10p10422.

Burchfiel, B.C., Cowan, D.S., and Davis, G.A., 1992, Tectonic overview of the Cordilleran orogen in the western United States, *in* Burchfiel, B.C., Lipman, P.W., and Zoback, M.L., eds., The Cordilleran Orogen: Conterminous U.S.: Boulder, Colorado, Geological Society of America, The Geology of North America, v. G-3, p. 407– 479, https:// doi .org /10 .1130 /DNAG -GNA -G3 .407.

Busby, C.J., Pavlis, T.L., Roeske, S.M., and Tikoff, B., 2023, The North American Cordillera during the Mesozoic to Paleogene: Selected questions and controversies, *in* Whitmeyer, S.J., Williams, M.L., Kellett, D.A., and Tikoff, B., eds., Laurentia: Turning Points in the Evolution of a Continent: Geological Society of America Memoir 220, p. 635–6 58, https:// doi .org /10 .1130 /2022 .1220 (31).

Busby- Spera, C.J., 1988, Speculative tectonic model for the early Mesozoic arc of the southwestern Cordilleran United States: Geology, v. 16, p. 1121– 1125, https:// doi .org /10 .1130 /0091 -7613 (1988)016 <3C1121: STMFTE>3E2 .3 .CO;2.

Carrivick, J.L., Smith, M.W., and Quincey, D.J., 2016, Structure from Motion in the Geosciences: West Sussex, UK, John Wiley and Sons, 197 p., https:// doi .org /10 .1002 /9781118895818.

Cawood, A.J., and Bond, C.E., 2018, eRock: An open-a ccess repository of virtual outcrops for geoscience education: GSA Today, v. 29, no. 2, p. 36– 37, https:// doi .org /10 .1130 /GSATG373GW .1.

Cichanski, M.A., 1995, Tectonic evolution of a portion of the Panamint Mountains, Death Valley, California [Ph.D. dissertation]: Los Angeles, University of Southern California, 109 p.

Cobb, J.A., 2015, Understanding the contractional history of Surprise Canyon, California through digital field mapping, 3D modeling, and geochronology [M.S. thesis]: El Paso, University of Texas at El Paso, 120 p.

Colomina, I., and Molina, P., 2014, Unmanned aerial systems for photogrammetry and remote sensing: A review: ISPRS Journal of Photogrammetry and Remote Sensing, v. 92, p. 79– 97, https:// doi .org /10 .1016 /j .isprsjprs .2014 .02 .013.

Davis, G.H., and Coney, P.J., 1979, Geologic development of the Cordilleran metamorphic core complexes: Geology, v. 7, p. 120–1 24, https://d oi.org/ 1 0.1130 / 0091-7613(1979) 7<120: G DOTCM>2 .0 .CO;2.

Davis, G.H., Reynolds, S.J., and Kluth, C.F., 2011, Structural Geology of Rocks and Regions (3rd edition): Hoboken, New Jersey, John Wiley & Sons, 864 p.

De Paor, D.G., 2016, Virtual rocks: GSA Today, v. 26, no. 8, p. 4– 11, https:// doi .org /10 .1130 /GSATG257A .1.

DeCelles, P.G., 2004, Late Jurassic to Eocene evolution of the Cordilleran thrust belt and foreland basin system,

western USA: American Journal of Science, v. 304, p. 105– 168, https:// doi .org /10 .2475 /ajs .304 .2 .105.
DeCelles, P.G., and Graham, S.A., 2015, Cyclical processes in the North American Cordilleran orogenic system: Geology, v. 43, p. 499– 502, https:// doi .org /10 .1130 /G36482 .1.
Delle Piane, C., Burlini, L., Kunze, K., Brack, P., and Burg, J.P., 2008, Rheology of dolomite: Large strain torsion experiments and natural examples: Journal of Structural Geology, v. 30, p. 767– 776, https:// doi .org /10 .1016 /j .jsg .2008 .02 .018.
Dunne, G.C., and Walker, J.D., 2004, Structure and evolution of the East Sierran thrust system, east- central California: Tectonics, v. 23, TC4012, https:// doi .org /10 .1029 /2002TC001478.
Fleming, Z., 2022, Using virtual outcrop models and Google Earth to teach structural geology concepts: Journal of Structural Geology, v. 156, https:// doi .org /10 .1016 /j .jsg .2022 .104537.
Fossen, H., and Cavalcante, G.C.G, 2017, Shear zones—A review: Earth-Science Reviews, v. 171, p. 434– 455, https:// doi .org /10 .1016 /j .earscirev .2017 .05 .002.
Furukawa, Y., and Hernandez, C. , 2015, Multi-v iew stereo: A tutorial: Foundations and Trends® in Computer Graphics and Vision , v. 9, no. 1– 2, p. 1– 148, http:// doi .org /10 .1561 /0600000052.
Harding, M.B., 1987, Geology of the Wildrose Peak area, Death Valley region, California [M.S. thesis]: Laramie, University of Wyoming, 196 p.
Hodges, K.V., Walker, J.D., and Wernicke, B.P., 1987, Footwall structural evolution of the Tucki Mountain detachment system, Death Valley region, southeastern California, *in* Coward, M.P., Dewey, J.F., and Hancock, P.L., eds., Continental Extensional Tectonics: Geological Society of London Special Publication 28, p. 393– 408, https:// doi .org /10 .1144 /GSL .SP .1987 .028 .01 .24.
Hodges, K.V., McKenna, L.W., Stock, J., Knapp, J., Page, L., Sternlof, K., Silverberg, D., Wüst, G., and Walker, J.D., 1989, Evolution of extensional basins and Basin and Range topography west of Death Valley, California: Tectonics, v. 8, p. 453–4 67, https://d oi.org/ 1 0.1029 / TC008i003p00453.
Hodges, K.V., McKenna, L.W., and Harding, M.B., 1990, Structural unroofing of the central Panamint Mountains, Death Valley region, southeastern California, *in* Wernicke, B.P., ed., Basin and Range Extensional Tectonics Near the Latitude of Las Vegas, Nevada: Geological Society of America Memoir 176, p. 377– 390, https:// doi .org /10 .1130 /MEM176 -p377.
Johnson, B.K., 1957, Geology of a part of the Manly Peak Quadrangle, southern Panamint Range, California: University of California Publications in Geological Sciences, v. 30, p. 353– 423.
Labotka, T.C., 1981, Petrology of an andalusite-t ype regional metamorphic terrane, Panamint Mountains, California: Journal of Petrology, v. 22, p. 261–2 96, https://d oi.org/ 1 0.1093 / petrology /22 .2 .261.
Labotka, T.C., Albee, A.L., Lanphere, M.A., and McDowell, S.D., 1980, Stratigraphy, structure, and metamorphism in the central Panamint Mountains (Telescope Peak quadrangle), Death Valley area, California: Geological Society of America Bulletin, v. 91, no. 3, Part II, p. 843– 933, https:// doi .org /10 .1130 /GSAB -P2 -91 - 843.
Labotka, T.C., Warasila, R.L., and Spangler, R.R., 1985, Polymetamorphism of the Panamint Mountains, California: A ^{39}Ar-^{40}Ar study: Journal of Geophysical Research: Solid Earth, v. 90, p. 10,359– 10,371, https:// doi .org /10 .1029 /JB090iB12p10359.
Levy, M., and Christie-B lick, N., 1991, Tectonic subsidence of the early Paleozoic passive continental margin in eastern California and southern Nevada: Geological Society of America Bulletin, v. 103, p. 1590– 1606, https:// doi .org /10 .1130 /0016 -7606 (1991)103 <1590: TSOTEP>2 .3 .CO;2.
Lima, R.D., Prior, M.G., Stockli, D.F., and Hayman, N.W., 2018, Protracted heating of the orogenic crust in Death Valley, California, USA: Geology, v. 46, p. 315– 318, https:// doi .org /10 .1130 /G39865 .1.
Macdonald, F.A., Prave, A.R., Petterson, R., Smith, E.F., Pruss, S.B., Oates, K., Waechter, F., Trotzuk, D., and Fallick, A.E., 2013, The Laurentian record of Neoproterozoic glaciation, tectonism, and eukaryotic evolution in Death Valley, California: Geological Society of America Bulletin, v. 125, p. 1203– 1223, https:// doi .org /10 .1130 /B30789 .1.
Mahon, R.C., Dehler, C.M., Link, P.K., Karlstrom, K.E., and Gehrels, G.E., 2014, Geochronologic and stratigraphic constraints on the Mesoproterozoic and Neoproterozoic Pahrump Group, Death Valley, California: A record of the assembly, stability, and breakup of Rodinia: Geological Society of America Bulletin, v. 126, p. 652– 664, https:// doi .org /10 .1130 /B30956 .1.
Matthews, N.A., Noble, T.A., and Breithaupt, B.H., 2016, Close- range photogrammetry for 3-D ichnology: The basics of photogrammetric ichnology, *in* Falkingham, P.L., Marty, D., and Richter, A., eds., Dinosaur Tracks: The Next Steps: Bloomington, Indiana University Press, p. 29– 55.
McCaffrey, K.J.W., Feely, M., Hennessy, R., and Thompson, J., 2008, Visualization of folding in marble outcrops, Connemara, western Ireland: An application of virtual outcrop technology: Geosphere, v. 4, p. 588– 599, https:// doi .org /10 .1130 /GES00147 .1.
Miller, M.G., and Pavlis, T.L, 2005, The Black Mountains turtlebacks: Rosetta stones of Death Valley Tectonics: Earth-S cience Reviews, v. 73, p. 115–138 , https:// doi .org/ 10 .1016 /j .earscirev .2005 .04. 007.
Mrofka, D., and Kennedy, M., 2011, The Kingston Peak Formation in the eastern Death Valley region, *in* Arnaud, E., Halverson, G.P., and Shields-Z hou, G., eds., The Geological Record of Neoproterozoic Glaciations: Geological Society of London Memoir 36, p. 449–4 58, https:// doi .org /10 .1144 /M36 .40.
Nelson, L.L., Smith, E.F., Hodgin, E.B., Crowley, J.L., Schmitz, M.D., and Macdonald, F.A., 2020, Geochronological constraints on Neoproterozoic rifting and onset of the Marinoan glaciation from the Kingston Peak Formation in Death Valley, California (USA): Geology, v. 48, p. 1083– 1087, https:// doi .org /10 .1130 /G47668 .1.
Norton, I., 2011, Two- stage formation of Death Valley: Geosphere, v. 7, p. 171– 182, https:// doi .org /10 .1130 /GES00588 .1.
Pavlis, T.L., and Mason, K.A., 2017, The new world of 3D geologic mapping: GSA Today, v. 27, no. 9, p. 4– 10, https:// doi .org /10 .1130 /GSATG313A .1.
Pavlis, T.L., and Serpa, L.F., 2023, Accuracy of Structure-f rom- Motion/Multiview Stereo terrain models: A practical assessment for applications in field geology: Geosciences, v. 13, 217, https:// doi .org /10 .3390 /geosciences13070217.
Pavlis, T.L., Langford, R., Hurtado, J., and Serpa, L., 2010, Computer- based data acquisition and visualization systems in field geology: Results from 12 years of experimentation and future potential: Geosphere, v. 6, p. 275– 294, https:// doi .org /10 .1130 /GES00503 .1.
Pavlis, T.L., Rutkofske, J., Guerrero, F., and Serpa, L.F., 2014, Structural overprinting of Mesozoic thrust systems in eastern California and its importance to reconstruction of Neogene extension in the southern Basin and Range: Geosphere, v. 10, p. 732–7 56, https:// doi .org /10 .1130 /GES00993 .1.
Petterson, R., Prave, A.R., Wernicke, B.P., and Fallick, A.E., 2011, The Neoproterozoic Noonday Formation, Death Valley region, California: Geological Society of America Bulletin, v. 123, p. 1317– 1336, https:// doi .org /10 .1130 /B30281 .1.
Platte, J.P., Behr, W.M., and Cooper, F.J., 2015, Metamorphic core complexes: Windows into the mechanics and rheology of the crust: Journal of the Geological Society, v. 172, p. 9- 27, https:// doi .org /10 .1144 /jgs2014 - 036.
Prave, A.R., 1999, Two diamictites, two cap carbonates, two δ^{13}C excursions, two rifts: The Neoproterozoic Kingston Peak Formation, Death Valley, California: Geology, v. 27, p. 339– 342, https:// doi .org /10 .1130 /0091 -7613 (1999)027 <0339: TDTCCT>2 .3 .CO;2.
Ramsay, J.G., 1967, Folding and Fracturing of Rocks: New York, McGraw- Hill, 568 p.
Ramsay, J.G., 1980, Shear zone geometry: A review: Journal of Structural Geology, v. 2, p. 83–9 9, https:// doi .org /10 .1016 /0191 -8141 (80) 90038-3.
Ramsay, J.G., and Graham, R.H., 1970, Strain variation in shear belts: Canadian Journal of Earth Sciences, v. 7, p. 786– 813, https:// doi .org /10 .1139 /e70 - 078.
Rutkofske, J.E., Pavlis, T.L., and Ramirez, S., 2022, Applications of modern digital mapping systems to assist inclusion of persons with disabilities in geoscience education and research: Journal of Structural Geology, v. 161, https:// doi .org /10 .1016 /j .jsg .2022 .104655
Snyder, N.P., and Hodges, K.V., 2000, Depositional and tectonic evolution of a supradetachment basin: ^{40}Ar/^{39}Ar geochronology of the Nova Formation, Panamint Range, California: Basin Research, v. 12, p. 19– 30, https:// doi .org /10 .1046 /j .1365 -2117 .2000 .00108 .x.
Stevens, C.H., and Stone, P., 2005, Interpretation of the Last Chance thrust, Death Valley region, California, as an Early Permian décollement in a previously deformed shale basin: Earth- Science Reviews, v. 73, p. 79–1 01, https:// doi .org /10 .1016 /j .earscirev .2005 .04 .005.
Stevens, C.H., Stone, P., and Kistler, R.W., 1992, A speculative reconstruction of the middle Paleozoic continental margin of southwestern North America: Tectonics, v. 11, p. 405– 419, https:// doi .org /10 .1029 /91TC02884.
Stevens, C.H., Stone, P., and Magginetti, R.T., 2015, Regional implications of new chronostratigraphic and paleogeographic data from the Early Permian Darwin Basin, east- central California: Stratigraphy, v. 12, p. 149– 166, https:// doi .org /10 .29041 /strat .12 .2 .05.
Subia, T.A., 2019, Ductile deformation in the central Panamint Mountains: A multi- disciplinary approach to a multi- dimensional problem [M.S. thesis]: El Paso, University of Texas at El Paso, 91 p.
Svennevig, K., Guarnieri, P., and Stemmerik, L., 2015, From oblique photogrammetry to a 3D model—Structural modeling of Kilen, eastern North Greenland: Computers & Geosciences, v. 83, p. 120– 126, https:// doi .org /10 .1016 /j .cageo .2015 .07 .008.

Tikoff, B., and de Saint Blanquat, M., 1997, Transpressional shearing and strike-s lip partitioning in the Late

Cretaceous Sierra Nevada magmatic arc, California: Tectonics, v. 16, p. 442– 459, https:// doi .org /10 .1029 /97TC00720.

Tirel, C., Brun, J.P., and Burov, E., 2008, Dynamics and structural development of metamorphic core complexes: Journal of Geophysical Research: Solid Earth, v. 113, B04403, https:// doi .org /10 .1029 /2005JB003694.

Trevino, S.F., and Tikoff, B., 2023, Two phases of Cretaceous dextral shearing recorded in the plutonic rocks of NW Nevada (USA): A tectonic link between intra-a rc shearing in the Sierra Nevada and Idaho batholiths: Geosphere, v. 19, p. 1539– 1564, https:// doi .org /10 .1130 /GES02682 .1.

Walker, J.D., 1988, Permian and Triassic rocks of the Mojave Desert and their implications for timing and mechanisms of continental truncation: Tectonics, v. 7, p. 685–7 09, https:// doi .org /10 .1029 /TC007i003p00685.

Walker, J.D., and Black, R.A., 2000, Mapping the outcrop: Geotimes, v. 45, no. 11, p. 28–3 1, http:// www.geotimes.org /nov00 /mapping.html.

Walker, J.D., Tikoff, B., Newman, J., Clark, R., Ash, J., Good, J., Bunse, E.G., Möller, A., Kahn, M., Williams, R.T., Michels, Z., Andrew, J.E., and Rufledt, C., 2019, StraboSpot data system for structural geology: Geosphere, v. 15, p. 533– 547, https:// doi .org /10 .1130 /GES02039 .1.

Wernicke B., and Burchfiel, B.C., 1982, Modes of extensional tectonics: Structural Geology, v. 4, p. 105- 115, https:// doi .org /10 .1016 /0191 -8141 (82) 90021-9.

Wernicke, B., Axen, G.J., and Snow, J.K., 1988, Basin and Range extensional tectonics at the latitude of Las Vegas, Nevada: Geological Society of America Bulletin, v. 100, p. 1738–1 757, https:// doi .org /10 .1130 /0016 -7606 (1988)100 <1738: BARETA>2 .3 .CO;2.

Wernicke, B., Snow, J.K., Hodges, K.V., Walker, J.D., Lahren, M.M., Trexler, J.H., and Spinosa, C., 1993, Structural constraints on Neogene tectonism, *in* Lahren, M.M., Trexler J.H., Jr., and Spinosa, C., eds., The Southern Great Basin: Crustal Evolution of the Great Basin and the Sierra Nevada: Geological Society of America Cordilleran/Rocky Mountain Sections Joint Meeting, Reno, Nevada, 1993, Field Trip Guidebook: Reno, Nevada, Mackay School of Mines, p. 453– 479.

Wernicke, B.P., Snow, J.K., Axen, G.J., Burchfiel, B.C., Hodges, K.V., Walker, J.D., and Guth, P.L., 1989, Extensional tectonics in the Basin and Range province between southern Sierra Nevada and the Colorado Plateau: 28th International Geological Congress Field Trip Guidebook T138, 80 p.

Westoby, M.J., Brasington, J., Glasser, N.F., Hambrey, M.J., and Reynolds, J.M., 2012, 'Structure- from- Motion' photogrammetry: A low- cost, effective tool for geoscience applications: Geomorphology, v. 179, p. 300–314, https:// doi .org /10 .1016 /j .geomorph .2012 .08 .021.

Whitmeyer, S., and Dordevic, M., 2023, A new tool for producing 3D orientation symbology for Google Earth: GSA Today, v. 33, no. 3– 4, p. 28– 29, https:// doi .org /10 .1130 /GSATG553GW .1.

Wilkinson, W.W., Jones, R.R., Woods, C.E., Gilment, S.R., McCaffrey, K.J.W., Kokkalas, S., and Long, J.J., 2016, A comparison of terrestrial laser scanning and structure- from- motion photogrammetry as methods for digital outcrop acquisition: Geosphere, v. 12, p. 1865– 1880, https:// doi .org /10 .1130 /GES01342 .1.

Wolf, P.R., and Dewitt, B.A., 2000, Elements of Photogrammetry with Applications to GIS (3rd edition): Boston, McGraw- Hill, 608 p.

Workman, J.B., Menges, C.M., Page, W.R., Taylor, E.M., Ekren, E.B., Rowley, P.D., Dixon, G.L., Thompson, R.A., and Wright, L.A., 2002, Geologic map of the Death Valley ground- water model area, Nevada and California: U.S. Geological Survey Miscellaneous Field Studies Map MF- 2381- A, scale 1:250,000, https:// doi .org /10 .3133 /mf2381A.

Wright, L.A., and Troxel, B.W., 1967, Limitations on right- lateral, strike- slip displacement, Death Valley and Furnace Creek fault zones, California: Geological Society of America Bulletin, v. 78, p. 933– 950, https:// doi .org /10 .1130 /0016 -7606 (1967)78 [933: LORSDD]2 .0 .CO;2.

Wright, L.A., Troxel, B.W., Williams, E.G., Roberts, M.T., and Diehl, P.E., 1976, Precambrian sedimentary environments of the Death Valley region, eastern California, *in* Troxel, B.W., and Wright, L.A., eds., Geologic Features—Death Valley, California: California Division of Mines and Geology Special Report 106, p. 7– 15.

Yonkee, W.A., and Weil, A.B., 2015, Tectonic evolution of the Sevier and Laramide belts within the North American Cordillera orogenic system: Earth- Science Reviews, v. 150, p. 531–5 93, https:// doi .org /10 .1016 /j .earscirev .2015 .08 .001.